Universität für Bodenkultur Wien
University of Natural Resources
and Life Sciences, Vienna

Master Thesis

Diffusion phenomena in protein adsorption on ion exchange chromatography media

Submitted by

Alexander MECHTLER, BSc

in the framework of the Master programme

Biotechnology

in partial fulfilment of the requirements for the academic degree

Diplom-Ingenieur

Vienna, September 2022

Supervisor:
Assoc. Prof. Dipl.-Ing. Dr. Rainer Hahn
Institute of Bioprocess Science and Engineering
Department of Biotechnology

Eidesstattliche Erklärung

Ich erkläre eidesstattlich, dass ich die Arbeit selbständig angefertigt, keine anderen als die angegebenen Hilfsmittel benutzt und alle aus ungedruckten Quellen, gedruckter Literatur oder aus dem Internet im Wortlaut oder im wesentlichen Inhalt übernommenen Formulierungen und Konzepte gemäß den Richtlinien wissenschaftlicher Arbeiten zitiert, durch Fußnoten gekennzeichnet bzw. mit genauer Quellenangabe kenntlich gemacht habe.

_____ _____

Wien, Datum Unterschrift

Acknowledgement

I would like to thank my supervisors Prof. Rainer Hahn and DI Jürgen Beck as well as the institute of bioprocess science and engineering for the opportunity of doing this thesis in their lab and the valuable input during the work.

I also want to address a thank you to all the members of the research group Hahn and the pilot plant core facility. Without their constant engagement and never-ending moral support, the completion of this project would not have been possible.

A special thanks I want to dedicate to my parents, grandparents as well as my sister for the constant trust and encouragement during all this time as well as the financial aid while working on this degree.

Gutta cavat lapidem non vi, sed saepe cadendo

(A water drop hollows a stone not by force, but by falling often)

Abstract

In this work, the adsorption of bovine serum albumin on four different anion exchange media (Q Sepharose Fast Flow, Q Ceramic HyperD F, Fractogel EMD TMAE Hicap (M) and Toyopearl GigaCap Q-650M) were investigated. The influence of various conditions like buffer composition, protein concentration and differences in linear chromatographic velocities were experimentally assessed. The intent was to investigate the dominating form of mass transfer and its dependencies as well as its limits under these conditions. For this, experimental frontal analysis data was established and modelled with pore, surface, or parallel diffusion models.

Breakthrough curve experiments with self-packed 0.5 mL LC columns revealed the impact of a strong binding buffer system onto the protein binding capacity, showing an increase of up to 2.5 times in capacity compared to weak binding buffer. These results were confirmed by adsorptions isotherm as well as batch adsorption experiments. The breakthrough curve experiments also indicated the mechanistic switch of surface to pore diffusion when changing from strong to weak binding buffer on Q Sepharose Fast Flow media. On pre-packed 0.2 mL LC columns from Repligen Corporation, these findings could be replicated, while the chromatographic linear velocity was increased up to 1000 cm/h. The evaluation of chromatographic modelling data revealed that Fractogel EMD TMAE Hicap (M) showed an increase of up to 4.5 times in its pore diffusion coefficient as in comparison to the free diffusivity D_0 of bovine serum albumin. This indicates a significant contribution of surface diffusion to the overall mass transfer on both buffer systems used. An increase of up to 3 times was found with the Toyopearl GigaCap Q-650M resin, leading to the same conclusion. For Q Sepharose Fast Flow weak binding buffer an effective pore diffusivity of $2.2*10^{-7}$ cm²/s and a solid diffusion coefficient of $1.5*10^{-8}$ cm²/s was derived from the determined apparent effective diffusion coefficient $\widehat{D_e}$. For the Q Sepharose Fast Flow strong binding buffer an apparent effective diffusion coefficient of $2.95*10^{-8}$ cm²/s was determined by an experimental approach based on a decrease in linear velocity u. Q-Ceramic HyperD showed a substantial trend towards a surface diffusion mechanism in all experiments, a standard surface diffusion coefficient D_s of $3*10^{-9}$ cm²/s for both buffer systems was derived and used for further predictions based on the linear chromatographic velocity. The iterative fitting approach for the parallel diffusion mechanism of Fractogel EMD TMAE Hicap (M) lead to predictions of the linear chromatographic velocity at 500 cm/h and 1000 cm/h.

The gained knowledge about the effect of triggering different mass transfer mechanism by solely changing the buffer or protein concentration will serve as basic information on diffusion behavior. Further on, it will aid in the establishment of multi component adsorption systems that rely on these findings. This will ultimately lead to more effective methods of chromatographic downstream processing in biotechnological production processes.

Zusammenfassung

In dieser Arbeit wird der Auswirkung der Adsorption von Rinderserumalbumin auf vier verschiedene Anionen Chromatographie Medien (Q Sepharose Fast Flow, Q Ceramic HyperD F, Fractogel EMD TMAE Hicap (M) and Toyopearl GigaCap Q-650M) untersucht. Der Einfluss von zahlreichen Einflüssen wie verschiedene Puffer Systeme, Protein Konzentrationen und der Einfluss der linearen chromatographischen Geschwindigkeit wird dahingehend untersucht. Der wissenschaftliche Hintergrundgedanke war das gültige Model des jeweiligen Massentransfers and seine Abhängigkeiten sowie die Limitationen zu evaluieren. Um dies durchzuführen, wurden experimentell ermittelte chromatographische Durchbruchskurven in Kombination mit Modellen der Poren, Oberflächen oder Paralleldiffusion verglichen.

Ergebnisse der chromatographische Durchbruchskurven, die mit selbst gepackten 0.5 mL Säulen durchgeführt wurden, zeigten den Einfluss eines starken bindenden Puffersystems auf die Proteinbindungskapazität. Es wurde eine um bis zu 2.5-fach erhöhter Bindungskapazität im Gegensatz zu den Ergebnissen des schwachen bindenden Puffersystems gemessen. Dieses Ergebnis wurden durch Adsorptions Isothermen sowie Batch Adsorptions Experimente bestätigt. Die Resultate der Durchbruchskurven deuteten außerdem auch einen mechanistischen Wechsel vom Oberflächen- zum Porendiffusionsmodell im Falle des Q Sepharose Fast Flow Mediums hin. An vorgepackten 0.2 mL LC Säulen der Firma Repligen wurden diese Ergebnisse bestätigt, es war in weiterer Folge möglich die chromatographische Geschwindigkeit auf bis zu 1000 cm/h an diesen zu erhöhen. Die Auswertung der Experimentellen Daten mittels chromatographischer Modellierung zeigte das die Porendiffusion des Fractogel EMD TMAE Hicap (M) Mediums im Vergleich zur Freien Diffusion von Rinderserumalbumin um den Faktor 4.5 angestiegen ist. Dies deutet darauf hin, dass der allgemeine Massentransport nicht alleinig mittels Porendiffusion bewerkstelligt wird, es dürfte bei beiden verwendeten Puffersystemen zusätzlich noch einen unbekannten Anteil an Oberflächendiffusion geben der dies fördert. Ein Anstieg um den Faktor 3 wurde bei Toyopearl GigaCap Q-650M gefunden, die selbige Erklärung dürfte auch hier gültig sein. Für das Q Sepharose Fast Flow schwach bindende Puffersystem wurde ein effektiver Poren Diffusion Koeffizient von $2.2*10^{-7}$ cm²/s, für die Oberflächen Diffusion ein Wert von $1.5*10^{-8}$ cm²/s aus dem experimentell bestimmten apparent effective diffusion coefficient $\widehat{D_e}$ berechnet. Für die Bestimmung des apparent effective diffusion coefficient des stark bindenden Puffersystems wurde ein Wert von $2.95*10^{-8}$ cm²/s mittels experimenteller Versuche, die auf einer reduzierten chromatographischen Geschwindigkeit *u* basieren, ermittelt. Ergebnisse des Q Ceramic HyperD F Resins zeigte eine Bestätigung des Oberflächendiffusions Models bei allen durchgeführten Experimenten. Ein Standard Oberflächendiffusion Parameter von $3.0*10^{-9}$ cm²/s wurde für beide Puffersysteme bestimmt und für Vorhersagen basierend auf der chromatografischen Geschwindigkeit verwendet. Ein iterativer Lösungsansatz zur Bestimmung der Paralleldiffusion Parameter, angewandt an Fractogel EMD TMAE Hicap (M), führte zu Vorhersagen, basierend auf einer chromatografischen Geschwindigkeit von 500 cm/h und 1000 cm/h.

Das gewonnene Wissen und die erworbene Erfahrung über den Effekt, wie verschiedene Mechanismen des Massentransfers nur durch ändern der Pufferbedingungen oder der Proteinkonzentration aktiviert werden können, wird als Grundlageninformation im Bereich der Chromatographischen Adsorption verwendet. Des Weiteren dient es als fundamentale Basis für die Implementierung eines Multi Komponenten Adsorptionssystems, das unter anderem auf den ermittelten Prinzipien fußt. Dies wird final zu effektiveren und effizienteren Methoden der Chromatographischen Produkt Aufreinigung in Biotechnologischen Produktionsprozessen führen.

Contents

1 Introduction

Over the course of the last decade biotechnology has proven to be one of the leading interdisciplinary fields of science. Having a positive impact on other sectors as the pharmaceutical industry, agriculture, chemicals as well as fuel and food production, its growth is steadily on the rise. A stable growth of 1.3% has been recorded between 2015 and 2020 worldwide.[1] However, it has been no secret at all that the industry is under pressure to constantly optimize existing methods or find new applications in need of meeting the global demand. Abrupt events like Covid-19 and its change to the global disease pattern have further proven that. An increased need for higher product quality and an enhanced purity of biotechnological products presses these requirements even further. Downstream processing unit operations are usually required for reaching this target. Chromatography has been the workhouse of downstream processing and its purification processes since the 1980s.[2] It is used in separation processes for proteins and allows for an excellent product cut-off as well as a high productivity. Ion exchange chromatography especially has proven to be quite reliable in these purification processes due to its mild conditions and cost efficiency. The solid-liquid protein mobility and distribution in these processes has a significant impact on the separation efficiency. It is therefore a general interest to generate a fundamental understanding of these transport phenomena to allow for a more efficient column adsorption, further increasing overall productivity. Usually, scouting experiments are performed on small scale columns to limit resin volume as well as the amount of sample used. This results in the overall cap of development costs. Lately chromatographic modelling has taken a big step up in the role of bioseparation. It allows for an in-silico approach to the complicated matter of chromatography, generating mechanistic models. These can simulate the complex manner of real time chromatography by a systematic approach if setup correctly. By creating a much more subtle, elegant, and efficient way of key bioprocess operation design, it allows to overcome the borders of conventional process development. The aim of modelling however is not to replace experimental setups, it is more aiming to supplement and support datasets that have been derived from laboratory results. In addition, the perimeter and boundaries of these mechanistic models must be determined to detect its limits.

This thesis aim was to investigate and put into perspective the different mechanisms of mass transfer effects under various small scale anion exchange chromatography conditions. These conditions include a weak and a strong binding buffer system and several different chromatographic resins with specific properties. The starting point for this research project was a publication done by Zhang et al.[3] They established the weak and strong binding buffer systems present in this thesis. Additionally, they did CLSM image experiments with BSA on several resins used in this thesis. It was set to confirm and extend these fundamental findings by doing frontal analysis chromatography experiments based on their conclusions. Subsequent, additional parameters were added step by step into the experimental design to enhance the overall picture of the underlying operating mass transfer mechanisms. The addition of parameter was done by varying the protein feed concentrations and the linear velocities *u* on the chromatographic system.
As a secondary aim of this study, simulations utilizing the Chromatography Analysis and Design Toolkit (CADET) were carried out. The simulation output is compared with the experimental results and reviewed. In addition, several calculations like the apparent effective diffusion coefficient $\widehat{D_e}$ were done before the simulations. These calculation results served as parameter inputs in the simulations and were tested against the experimental results. Finally, it is tested to what degree the pore diffusion coefficient and parallel diffusion coefficient ratio influence the parallel diffusion coefficient of certain experimental designs. This was done by iterative fitting of the experimental data.

2 Theory

2.1 Principles of liquid chromatographic separation

As the single most multipurpose unit operation in downstream separation processes, liquid chromatography (LC) has established itself as a major concept in the market of biopharmaceutical compound purification. Showcasing its versatility, it has proven to be suited for several fields of application. Variants of this versatility are known as ion exchange chromatography (IEX), hydrophobic interaction chromatography (HIC), size exclusion chromatography (SEC), affinity chromatography (AC), metal chelate chromatography (MCC) and the reversed phase chromatography (RPC)[4]. All these variants differ by their physical interaction forces. However, they are all based upon the most fundamental concept of chromatography, the interaction of a fixed (solid) phase with a mobile phase that moves through the stationary bed. The mobile to solid phase interaction is dependent on the interaction principle and can vary by pH, hydrophobicity, and ion strength. The stationary phase is case to subject, depending on the previously mentioned interaction methods and varying. The stationary phases are designed to fit toward the different modes of chromatographic separation, all providing a different mechanism correlating between the solute and the two phases. These mechanisms can be subdivided into different classes. Example for these classes are molecule size differences in the solute (SEC), differences in affinity (AC) or different electrostatic force strength of the target (IEC). It is also possible to combine two or more of the above-mentioned modes of separation, resulting in the mixed-mode chromatography (MCC). Usually, the stationary phase is packed in a fixed bed column to provide a better practical accessibility for the feed and the mobile phase. This procedure is known as column chromatography. The separation process is usually aimed towards the generation of a selective binding of the molecule of interest, although there exist several processes where the unhindered flowthrough is the product.

In liquid chromatography a variety of stationary phase materials has been established over the course of the years. The different requirements of developing a higher separation resolution, improved protein binding capacity and enhanced structural stability has led to a variety of different chromatographic resins. Most of these developed stationary phases are based on inorganic materials like silica, organic polymers, or polysaccharides. The particle size can usually vary from 2.5 µm up to 150 µm, they are all characterized by their bead shaped core that incorporates liquid filled pores. In those pores of < 100 nm transport takes places by diffusion. A packed bed of these beads in a column is defined by several types of porosities, they are all interconnected by Equation 2.1.

$$\varepsilon_t = \varepsilon + (1 - \varepsilon)\varepsilon_p \qquad 2.1$$

The extra-particle porosity ε varies over a given range, being independent from the particle size and can usually be assumed between 0.3 – 0.4. It is also known as void fraction and is defined as the volume between the packed particles. The intra-particle porosity ε_p being highly dependent on the particle structure varies over a much broader range. It represents the ratio of liquid-filled pores to the total volume of the bead particle. The total column porosity ε_t represents the sum of the extra-particle porosity ε and intra-particle porosity ε_p.
The separation behavior of these liquid chromatography resins however is not only defined by the material or the properties of the liquid-filled pore. Additionally, ligands are added to the particles, completing the resin, and enabling its full separation performance.

2.2 Ion exchange chromatography

IEX is one of the most frequent used chromatographical key technologies for the purification of proteins from pharmaceutical feed stocks. Its separation principle is based on the electrostatic separation on ionogenic groups. This molecular interaction requires coulombic forces between the different charged ionic species to be present. If these ionogenic resin ligands are positive charged the operational mode is called anion-exchange chromatography. If the resin has a negatively charge it is called cation-exchange chromatography. Typical resin ligands can be divided into several categories according to their charge and the strength of their charge, resulting in the subcategorization of strong and weak ion exchanger. Examples for strong cation-exchange resin ligands are sulfyl (S), sulfopropyl (SP) and methyl sulfonate (SM), while common weak cation-exchange ligands are carboxy (C) or carboxymethyl (CM). Quaternary aminoethyl (QAE), triethylaminoethyl (TEAE), or trimethyl aminoethyl (TAM) groups have proven to be reliable strong anion-exchange resin ligands while diethylaminoethyl (DAEA) or aminoethyl (AE) prove to be weak anion-exchange resin ligands. Example for the usage of this ligands can be found in the Sepharose Fast Flow series (Cytiva), Poros HQ (Applied Biosystems) or the UNOsphere series (Bio-Rad Laboratories). The amount of these ligands determines the overall ion exchange capacity, a common resin characteristic usually provided by the supplier. It is defined as the amount of acidic or basic groups per defined amount of ion exchanger. Common units for these are milliequivalent per weight dry exchanger or milliequivalent per volume of fully swollen exchanger. This total ionic ligand capacity is a constant that is not influenced by experimental conditions.

The ligand interaction with biomolecules is determined by the so-called net surface charge *z*. A biomolecule has a net surface charge that is pre-determined by its amino acid sequence. Amino acids can either have an acidic or a basic residue that will influence the net protein charge of the protein. In case the net surface charge *z* of the protein is zero, all amino acids of the protein are in an uncharged state. The change of charge can be mediated by the pH or other environmental influences. When a net surface charge *z* of zero has been reached, the corresponding pH is then called isoelectric point *pI*. If a pH has been reached that is lower than the corresponding isoelectric point, the protein is positive charged and vice versa.

In IEX the net charge of the protein is adjusted by the sample buffer, this assists in helping to prepare the protein for the ion exchange strategy. The usual aim is to generate a most preferred binding of the protein with the resin ligands. The preference of this binding is defined by the selectivity, which plays an important role in the design of separation strategies. The selectivity is defined as the ability of an ion exchanger to choose a specific counter ion over another and caused by several physical phenomena. After applying the sample to the column all impurities and non-bound residues can be found in the flowthrough. Elution of the bound protein is usually done by increasing the overall salt concentration in the chromatography feed, leading to a replacement of the protein in benefit of the more favored Na^+ and Cl^- counter ions. The intensity of this competing mechanism can be used to elute differently charged protein selectively. A weaker charged proteins is usually eluted with a lower counter ion concentration than stronger charged proteins. These requires a much more higher counter ion concentration. An alternative elution by changing the pH of the feed elution is also a common procedure. However, this might trigger a denaturation of the protein structure and would probably conclude in the need of an additional protein refolding step.

2.2.1 Polymer functionalized media

A noteworthy type of ion exchange resins was developed by utilizing a composite type of matrix, the polymer functionalized media resins. These offer a significant change from the previously conventional bead like structured resins by utilizing functionalized monomers or polymers. The functionalized groups are anchored to the composite matrix surface by either a single- or multi- point attachment. As there are different types of polymers composite media, they can be divided into different classes.[5-7] The first class consists of resins that offer polymer binding by either introducing a covalent bound to a surface extender or graft polymerization to the backbone. Examples for this are the Sepharose XL (Cytica), Capto (Bio-Rad Laboratories) and GigaCap (Tosoh Bioscience) as well as the Fractogel EMD series (Merck Millipore). The second class are the so called 'gel-in-a-shell' media. They consist of a rigid particle, which pores are filled up by a cross-linked gel structure that is charged. Noteworthy representatives for these grafted types are Ceramic HyperD (Pall Bioscience) and UNOsphere (Bio-Rad Laboratories)
Figure 1 represents the typical build-up of such graft polymer functionalized media particle. The graph was taken from The Column blog provided by Thermo Fisher Scientific[8] and edited by the thesis author to provide a better understanding of the pictured case.

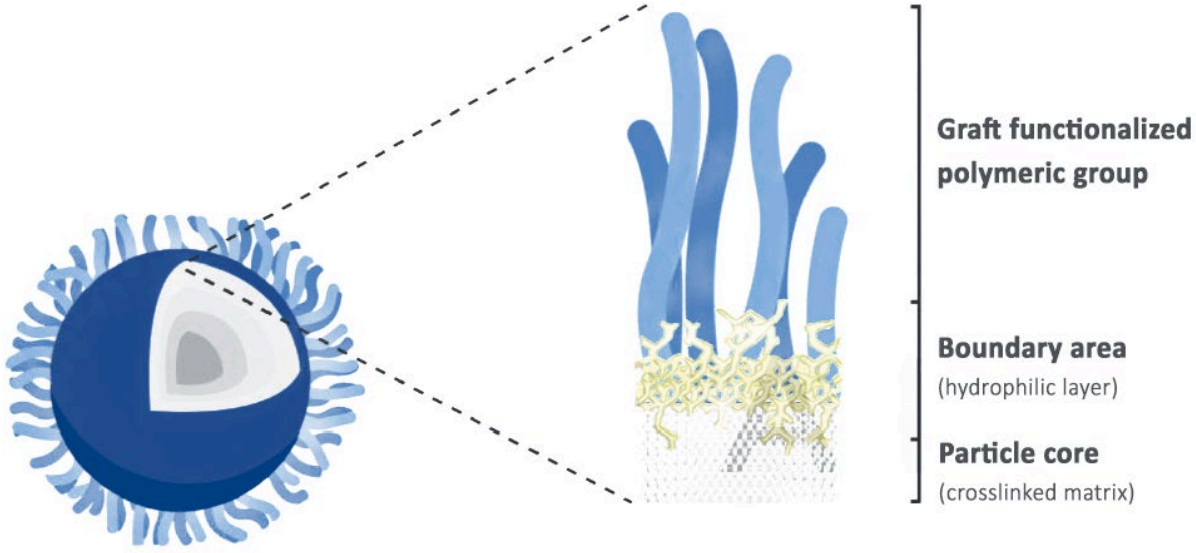

Figure 1: Schematic illustration for the case of a covalently bound monomer grafted to a crosslinked particle core. On the left a whole resin particle with its tentacle like structure anchored on the outside can be seen. On the right a more detailed picture of the binding structure is depicted. The size of polymer chains, the hydrophilic layer and the whole particle do not represent their actual size

In some cases, a spacer is utilized to enhance the performance of the functionalized polymers due to improved 3D architecture of the functionalized polymer that benefits steric effects. In this case a compromise must be made for the spacer length to avoid wall effects, a too short spacer however might trigger a hindered diffusional behavior of the target protein. If the spacer is too long there might be a performance drop off due to loosening effects[9].
The polymer functionalized media resins are known to show a significant improvement in mass transfer kinetics and protein binding capacity in comparison to their porous particle counterparts due to the application of enhanced mass transfer mechanics.

2.3 Mass transfer mechanics

2.3.1 Adsorption equilibria

The adsorption process of proteins on the stationary phase in equilibrium is described via adsorption isotherms. A common approximation model, which is used quite often to describe these adsorption processes is the Langmuir adsorption isotherm mode. It was originally designed to describe gas adsorption processes on inorganic surfaces and is expressed via:

$$q = \frac{q_m\, K\, C}{1 + K\, C} \tag{2.2}$$

q_m is the maximum concentration of the adsorbed solute, K is known as the equilibrium constant of the adsorption process, C the concentration of the solute. It also is possible to write the Langmuir isotherm with the dimensionless separation factor R:

$$R = \frac{1}{1 + K\, C_{ref}} \tag{2.3}$$

C_{ref} is usually stated as the initial concentration of the protein. For $R = 1$ the Isotherm is considered linear, favorable for $R < 1$, and rectangular for $R > 1$. The Langmuir model focuses on a monolayer formation of the solute onto the stationary phase. The maximum available binding capacity is dependent on the available surface area as well as the number of available binding sites.

In bioseparation processes usually not only one species is present in the bulk fluid. There are a variety of components that are encountered in practical bio-chromatography purification scenarios. The extension of the Langmuir Isotherm from Equation 2.3 is used for multicomponent systems. It is valid for a variety of N- adsorbed solutes and practically described by Butler and Ockrent[10] as well as Markham and Benton[11]:

$$q_i = \frac{q_m\, K_i\, C_i}{1 + \sum_{j=1}^{N} K_j\, C_j} \tag{2.4}$$

Whereas K_i q_i and C_i are the adsorption equilibrium constant, maximum binding capacity and concentration of the corresponding component for all variants of i. A more advanced model, that is used in protein adsorption on ion-exchangers, describes the retention mechanisms present in protein uptake equilibria is the steric mass action (SMA) model. It was proposed by Books and Cramer[12] and is an advancement to the stoichiometric displacement (SD) model it is initially based on. The SMA model key introduces the shielding constant σ to account for steric hindrance effects caused by the size of the molecule and can be written in the following isotherm expression:

$$q = \frac{K_e\, [q_0 - (z + \sigma)q]^z\, C}{(C_{Na^+})^2} \tag{2.5}$$

Whereas K_e is known as the dimensionless equilibrium constant, z is the protein effective charge, q_0 denotes the resin charge density, σ the number of blocked ligands, C has been used as the concentration of the fluid phase and C_{Na^+} being defined as the number of Na^+ counterions being exchanged in the process. The determination of the maximum protein binding capacity is simplified and can be assumed using the following expression:

$$q_{max} = \frac{q_0}{z + \sigma} \tag{2.6}$$

2.3.2 Adsorption kinetics

The molecules in the mobile phase are transported in between the particle beads through the bed by convective flow. The transport process of the solute into the small stationary phase pores occurs by diffusion. The solute saturation of the liquid-filled pores leads to the build-up of a concentration gradient $C_p - C_{p,s}$ whereas C_p is the concentration of solute in the bulk fluid and $C_{p,s}$ the protein concentration at the particle surface. This gradient acts between the stationary phase and the mobile phase in the interstitium. The diffusional transport goes hand in hand with several transport resistances that influence the diffusional behavior. Figure 2 gives an overview over these resistances.

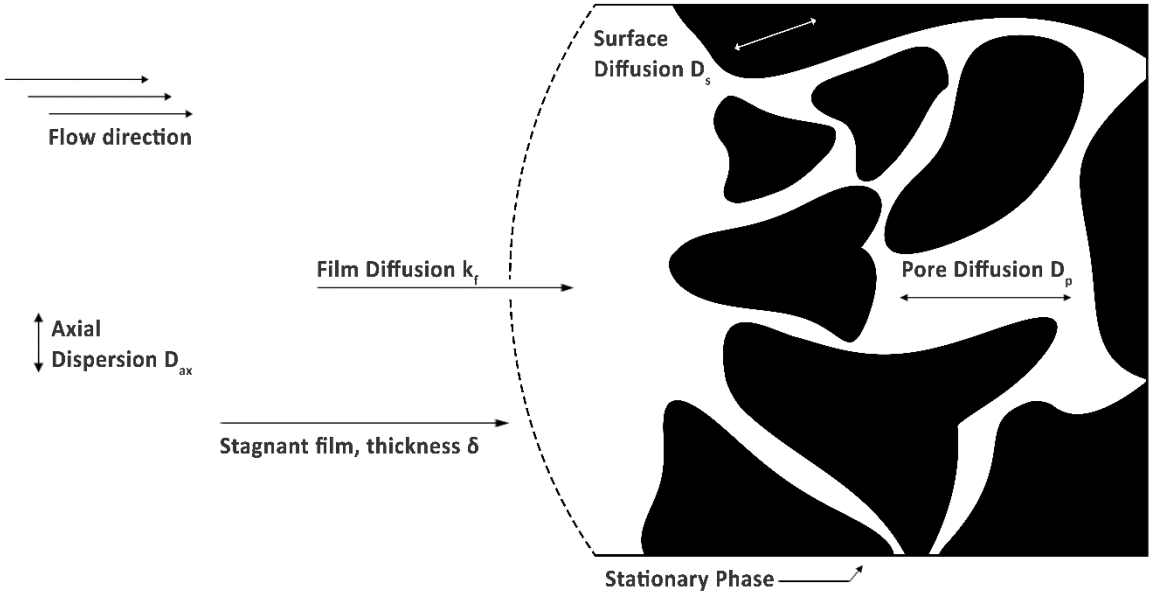

Figure 2: Sketch illustration of transport and kinetic resistances onto a particle. The different effects of stagnant film, film diffusion, axial dispersion, surface diffusion and pore diffusion are displayed in the graph. Flow direction is from left to the right.

Axial Dispersion D_{ax} is the sum of axial diffusion and complex hydrodynamic dispersion effects that appear when the mobile phase enters the extra-particle space. This causes the appearance of a non-uniform flow profile. The axial dispersion D_{ax} is dependent on operation conditions and subject of advanced calculation to simulate the realistic conditions in non-uniform flow profiles. According to Altenhöner and coworkers[13] it can be simplified as follows:

$$D_{ax} = HETP\ \frac{u}{2} \tag{2.7}$$

With u being the interstitial velocity inside the column and the HETP known as the Height Equivalent to a Theoretical Plate. The HETP can be calculated from experimental data using the first momentum μ and the second momentum σ. L is destined as the length of the column.

$$HETP = \frac{\sigma^2}{\mu^2}\ L \tag{2.8}$$

The Film diffusion coefficient displayed in Figure 2 is going to be discussed in detail in Section 2.3.2.1. The pore and surface diffusion mechanisms are further explained in Section 2.3.2.2.1 and Section 2.3.2.2.2.

All these effects appearing on different molecular scales can be comprehended using the General Rate Model (GRM)[14-18]. It is a most comprehensive model and depicts a detailed approach used in liquid

chromatography operations to consider the real conditions and effects present in a packed bed. It has been simplified several times, examples for this are the transport dispersive (TD)[19] or the equilibrium dispersive (ED)[20] model.

Its main assumptions are that only the axial coordinates in the column and the radial coordinates in the beads are considered, their impact on chromatographic band broadening is neglected. The transport of solute molecules through the insterstitial column by convective flow, band broadening caused by axial dispersion and mass transfer resistance through a stagnant film onto the particle are described in Equation 2.9 by a partial differential equation established by von Lieres[18]:

$$\frac{\partial c_p}{\partial t} = -u\frac{\partial c_p}{\partial \mathrm{z}} + D_{ax}\frac{\partial^2 c_p}{\partial \mathrm{z}^2} - \phi\frac{3}{r_p}k_f\left(c_p - c_{p,i}\right) \qquad 2.9$$

c_p is the concentration of a solute in the bulk fluid, $c_{p,i}$, is known as the solute concentration in the pore liquid, t denotes the time coordinate, u the interstitial velocity of the system, z the axial coordinate in the column, D_{ax} the axial dispersion coefficient, ϕ the phase ration, specified by $\phi = (1 - \varepsilon)/\varepsilon$ (ε *is* the extra-particle porosity mentioned in Section 2.1), r_p the radius of the particle and k_f is the film mass transfer diffusion coefficient.

2.3.2.1 External mass transfer

External mass transfer resistance is described by the film mass transfer coefficient k_f in Equation 2.9:

$$J = k_f(C_p - C_{p,s}) \qquad 2.10$$

Whereas J is the mass transfer flux at the particle surface, C_p is the concentration of solute in the bulk fluid and $C_{p,s}$ the protein concentration on the particle surface. For steady state conditions over a thin, stagnant film the following is valid:

$$\delta = \frac{D_0}{k_f} \qquad 2.11$$

δ is the thickness of the stagnant film mentioned in Figure 2, it is affected by the hydrodynamic conditions outside of the particle; D_0 is the free diffusivity of the molecule, it is more detailed explained in Section 2.3.2.2.1. The film mass transfer coefficient increases with higher particle size and lowering fluid velocities, it is practically estimated using the Carberry correlation[21]:

$$k_f = 1.15\frac{u}{\varepsilon^{1/2}}Re^{-1/2}Sc^{-2/3} \qquad 2.12$$

u is the superficial velocity in the column, ε the extra-particle porosity mentioned in Section 2.1, *Re* is known as the Reynolds number, *S*c the so-called Schmidt number. They are general engineering correlations for mass transfer coefficients in packed bed adsorptions and defined as following:

$$Re = u\frac{d_p}{\nu} \qquad 2.13$$

$$Sc = \frac{\nu}{D_0} \qquad 2.14$$

d_p is known as the particle diameter, ν denotes as the kinematic viscosity, D_0 is the free diffusivity of the molecule.

2.3.2.2 Intraparticle diffusion

The general diffusional transport for spherical particles using these influences is described by the following model:

$$\varepsilon_p \frac{\partial c}{\partial t} + \frac{\partial q}{\partial t} = \frac{1}{r^2}\frac{\partial}{\partial \mathrm{r}}\left[r^2\left(\varepsilon_p D_p \frac{\partial \mathrm{c}}{\partial \mathrm{r}} + D_s \frac{\partial \mathrm{q}}{\partial \mathrm{r}}\right)\right] \quad 2.15$$

For boundary conditions:

$$t = 0 : c = 0; q = 0; r = 0: \frac{\partial \mathrm{c}}{\partial \mathrm{r}} = 0 \quad 2.15a$$

$$r = r_p: \varepsilon_p D_p \frac{\partial c}{\partial r} + D_S \frac{\partial q}{\partial r} = k_f\left(c_p - c_{p,i}\right) \quad 2.15b$$

With c_p defined as the concentration of a solute in the bulk fluid and $c_{p,i}$, being known as the solute concentration in the pore liquid. D_e is known as the pore diffusion coefficient and D_s as the solid or surface diffusion coefficient. ε_p has been defined in Equation 2.1 as the intra-particle porosity, r_p is the particle radius and k_f the film mass transfer coefficient. Equation 2.15 describes a case where pore and surface diffusion both contribute to the mass transfer at the same time, the so-called parallel diffusion model. The Pore diffusion model can be expressed when using $D_s = 0$ in the above-mentioned equation, the surface diffusion model when substituting $D_p = 0$.

2.3.2.2.1 Pore diffusion model

Pore diffusion describes the transport process of solutes that tend to diffuse in large enough pores without any interaction of the force field constructed by the pore walls. Pore Diffusion usually is expressed by an effective pore diffusivity D_e, the protein mass transfer flux in the stationary phase is given by:

$$J = -D_e \nabla_c \quad 2.16$$

Hereby ∇_c is defined as the protein concentration gradient in the pore liquid. D_e is the effective pore diffusivity. It can be rewritten in the more detailed form of:

$$D_e = \frac{\varepsilon_p\, D_0}{\tau_p}\, \psi_P \quad 2.17$$

Whereas the parameters of the equation are defined as intra-particle porosity ε_p, D_0 is the free diffusivity of the molecule, τ_p the tortuosity factor and ψ_P as the diffusional hindrance coefficient. The tortuosity factor τ_p considers the random distributed orientation within the intra-particle pores. The available path is not considered as straight, it can be assumed as labyrinth like and extends therefore to a greater amount in total length that must be considered. Values for the tortuosity factor τ_p usually are between 1.5 and 4 in protein chromatographic assumptions.

The diffusional hindrance coefficient ψ_P is influenced by the steric size exclusion of the diffusional molecule. The molecule of interest cannot overcome the pore of a resin at a distance closer than the appropriate molecular radius. It is also affected by the physical phenomena of viscous drag or hydrodynamic resistance forces. These forces are based on the colloidal representation of a biological molecule that is moved inside an idealized cylindrical pore. The diffusional hindrance coefficient ψ_P is dependent on the ratio of hydrodynamic protein radius to resin pore radius λ_m. In literature[22; 23] it is defined as following:

$$\psi_P = \left(1 + \frac{9}{8}\lambda_m \ln \lambda_m - 1.539\,\lambda_m\right) \quad for\ \lambda_m < 0.2 \tag{2.18}$$

$$\psi_P = 0.865\,(1-\lambda_m)^2\left(1 - 2.1044\,\lambda_m + 2.089\,{\lambda_m}^3 - 0.984\,{\lambda_m}^5\right) \quad for\ \lambda_m > 0.2 \tag{2.19}$$

With the ratio of hydrodynamic protein radius to resin pore radius λ_m being defined as:

$$\lambda_m = \frac{r_h}{r_{pore}} \tag{2.20}$$

D_0 from Equation 2.17 is known as the free diffusivity, it is often also referred to as molecular diffusion coefficient or diffusivity in solution. D_0 is determined by the empirical calculation from Stokes-Einstein equation and depends on temperature, the size of the target as well as the viscosity of the medium. Unlike to its name it has been elaborated by Bird et al[24] on the principal groundwork by Einstein in continuum fluid mechanics and the movement of spherical particles in fluids.

$$\frac{D_0\,\eta}{T} = \frac{k_B}{6\,\pi\,r_h} \tag{2.21}$$

The free diffusivity D_0 in Equation 2.21 is expressed via the Boltzmann constant k_B, the hydrodynamic radius r_h, the temperature T as well as the dynamic viscosity η. This equation has been known to get modified in the past, one notable adaption by Tyn and Gusek[25] should be mentioned here among various others. It is valid for globular proteins in its shortened form.

$$\frac{D_0\,\eta}{T} = \frac{9.2\times10^{-8}}{(M_r)^{1/3}} \tag{2.22}$$

The calculation of the model as a method to determine the diffusion parameter is done by fitting the appropriate experimental generated curve data to calculated data from the pore diffusion model using the constant pattern solution of Weber et al.[26]. This model was further sophisticated by the works of Carta et al [27].

The following equation uses the solution that is valid for constant pattern conditions ($N\tau_1 > 2.5$):

$$\begin{aligned}(\tau_1 - 1)N_{pore} = {} & \frac{15}{\sqrt{3}}\tan^{-1}\left[\frac{2\left(1-\frac{C}{C_F}\right)^{1/3}+1}{\sqrt{3}}\right] \\ & -\frac{15}{2}\ln\left[1+\left(1-\frac{C}{C_F}\right)^{\frac{1}{3}}+\left(1-\frac{C}{C_F}\right)^{\frac{2}{3}}-\frac{1}{3}\right]+\frac{N_{pore,F}}{N_{film}}(\ln Y+1)-\frac{5\pi}{2\sqrt{3}}\end{aligned} \tag{2.23}$$

With condition:

$$(\tau_1 - 1) \geq \frac{5}{2} + \frac{N_{pore,F}}{N_{film}} \tag{2.23a}$$

Where:

$$\frac{N_{pore,F}}{N_{film}} = \frac{5\,D_e}{k_f\,r_p} \tag{2.24}$$

$$N_{pore} = \frac{15\,(1-\varepsilon)\,D_e\,L}{u\,{r_p}^2} \tag{2.25}$$

$$\tau_1 \, N_{pore} = (\tau_1 - 1) N_{pore} + N_{pore} \qquad 2.26$$

$Y = C / C_p$ is the dimensionless concentration of the system, with C / C_p being defined as the current protein concentration per maximum feed protein concentration, L is the length of the column, $N_{pore,F}$ is considered as the number of transfer units in the pore, N_{film} is accounted as the number of transfer units on the film, τ_1 is the dimensionless time, all other needed parameters have been denoted in previous mentions of Section 2.3.2. The protein load per column volume is calculated according to the following equations:

$$\frac{mg\ protein\ load}{mL\ column} = \frac{t_{abs}\, t_{scale}\, u\, C_p}{L} \qquad 2.27$$

$$t_{abs} = \frac{\frac{L\,\varepsilon}{u} + \frac{\tau_1\, N_{pore}\, {r_p}^2}{15\, D_e} \frac{q_m}{C_F}}{t_{scale}} \qquad 2.28$$

With t_{scale} = 1, u known as the linear velocity, C_p the used protein concentration, q_m as the protein binding capacity and D_e being the pore diffusion coefficient.

2.3.2.2.2 Surface diffusion model

Due to reasons like sterical hindrance, physical repulsion in the pore, size exclusion of the molecule or enhanced attraction towards the surface, pore diffusion may not always be the dominating mass transfer. An alternative transport mechanism that is based on transport in absorbed states without attachment is distinguished by an effective solid phase diffusivity D_s. The magnitude of D_s is usually 10 – 10^2 smaller than the pore diffusion D_e for proteins.

An analytical solution of the packed bed equation, that considers external film resistance, has been developed by Yoshida et al[28] and further sophisticated by Carta et al[29]. The final model consists of 2 graphical outputs (curves), which must be calculated separately. To generate a full prediction or fit of the data bot curves need to be displayed in a single graph together.

For lower curve part:

$$\frac{C}{C_F} = \frac{1}{\delta} \exp\left(\tau - \zeta + \delta - 1 - \frac{1}{\delta}\right) \qquad 2.29$$

With condition:

$$\tau - \zeta \leq -\delta + 1 + \frac{1}{\delta} - \ln\left(\frac{1+\delta}{\delta}\right) \qquad 2.29a$$

For upper curve part:

$$\frac{C}{C_F} = 1 - \frac{1}{1+\delta} \exp\{[-\tau + \zeta + 1 - \ln(1+\zeta)/\zeta]\} \qquad 2.30$$

With condition:

$$\tau - \zeta \geq 1 - \ln(1+\delta) \qquad 2.30a$$

Whereas time parameter τ, diffusion resistance parameter δ and bed length parameter ζ are defined as following:

$$\tau = \frac{6\,k_f}{d_p}\,\frac{c_F}{q_m}\left[t - \left(\frac{\varepsilon\,L}{u}\right)\right] \tag{2.31}$$

$$\delta = \frac{1}{10}\frac{k_f\,d_p}{D_s}\frac{c_F}{q_m} \tag{2.32}$$

$$\zeta = \frac{6\,(1-\varepsilon)}{d_p}\frac{k_F\,L}{u} \tag{2.33}$$

With D_s being defined as the surface diffusion coefficient, all other needed parameters have been denoted in previous mentions of Section 2.3.2.

For values of $\delta \leq 1$ the solution of Vermeulen et al.[30] is advised, for $\delta > 10$ the solution of Cooper et al.[30] is recommended. Calculation of film mass transfer k_f is according to Equation 2.12 (Carberry equation).

2.3.2.2.3 Parallel diffusion model

As in Equation 2.15 - Equation 2.15b denoted, the parallel diffusion model describes a case where both pore diffusion and surface diffusion model have contributing effects onto the mass transport flux. An approximate general expression for mass transfer flux in terms of overall effective pore diffusivity while breaking down the influence of both diffusional variables is offered by:

$$\widehat{D_e} = D_e + D_s\frac{q_m}{c} \tag{2.34}$$

This equation represents the so-called apparent effective diffusion coefficient, $\widehat{D_e}$. When enhancing the effective pore diffusivity D_e expressed in Equation 2.17 with the intraparticle porosity ε_p, the effect of the intraparticle diffusivity D_p becomes visible:

$$D_e = D_p\varepsilon_p \tag{2.35}$$

Combining Equation 2.34 with Equation 2.35 leads to:

$$\widehat{D_e} = D_p\varepsilon_p + D_s\frac{q_m}{c} \tag{2.36}$$

2.3.2.3 Batch Adsorption

As a particular useful method to quantify mass transfer rates of biomolecules onto particles, batch adsorption has been established. It offers a quick way of determining the adsorption kinetics of different adsorbents on lab scale. The simplest type of batch adsorption setup contains a stirred vessel with the particles of interest adjusted to a defined concentration. Onto the particle suspension, a protein solution is added, and samples are drawn at pre-defined time points. The reaction in these samples is stopped and the remaining protein concentration is measured by UV/VIS spectroscopy. The batch adsorption method therefore shares certain characteristics with a time course method.

2.3.2.3.1 Pore diffusion model

For a rectangular isotherm, the pore diffusion model involves film diffusion and pore diffusion control. This is however only valid for a R < 0.1 from Equation 2.3, in that case the isotherm is favorable. The model was developed by Weaver and Carta[29] and can be expressed using the following analytical solution:

$$\frac{C_p}{q_m}\frac{D_e\,t}{r_{p^2}} = \left(1 - \frac{1}{Bi}\right) I_1 - I_2 \qquad 2.37$$

Where:

$$I_1 = \frac{1}{6\,\lambda\,\Delta}\ln\left[\frac{\lambda^3 + \eta\,(\lambda+1)^3}{\lambda^3 + 1\,(\lambda+\eta)}\right] + \frac{1}{\lambda\,\Delta\,\sqrt{3}}\left[\tan^{-1}\left(\frac{2\,\eta - \lambda}{\lambda\,\sqrt{3}}\right) - \tan^{-1}\left(\frac{2-\lambda}{\lambda\,\sqrt{3}}\right)\right] \qquad 2.38$$

$$I_2 = \frac{1}{3\,\Delta}\ln\left(\frac{\lambda^3+\eta}{\lambda^3+1}\right) \qquad 2.39$$

With:

$$\Delta = \frac{V_P\,q_m}{V\,C_p} \qquad 2.40$$

$$\lambda = \left(\frac{1}{\Delta} - 1\right)^{\frac{1}{3}} \qquad 2.41$$

$$\eta = (1-F)^{\frac{1}{3}} \qquad 2.42$$

$$Bi = \frac{k_f\,r_p}{D_e} \qquad 2.43$$

$$F = \frac{q}{q_m} \qquad 2.44$$

$$V_P = V_{\,M}(1-\varepsilon) \qquad 2.45$$

C_p being the protein concentration, V_p is known as the particle resin volume, V_M as the volume of resin that was actually used for the experiment, V denotes the volume that was used for the solution, *Bi* the Biot number and *F* being the dimensionless fractional equilibrium approach of the system.

2.3.2.3.2 Surface diffusion model

Surface diffusion influence can be calculated via the Homogeneous Diffusion model with assumed intraparticle mass transfer control. The driving force is expressed via the adsorbed solute concentration within the particles. It is not dependent on film mass transfer control, and valid for a rectangular isotherm. The model is given via the following analytical expression by Helfferich and Plesset[31] for the entire range of F:

$$F = \sqrt{1 - exp(\pi^2 * (-\tau_D + 0.96 * \tau_D^2 - 2.92 * \tau_D^3))} \qquad 2.46$$

With:

$$\tau_D = \frac{D_s * t}{r_p^2} \qquad 2.47$$

D_s is denoted as the surface diffusion coefficient, r_p as the particle radius and *t* as the time variable for the system.

2.4 Breakthrough curve

A frontal analysis run is an experimental setup where the bulk solution is continuously applied to the column until it is overloaded, and feed begins to break through the column. This so-called breakthrough contains unbound protein as well as all other impurities and components that have been applied with the feed from the beginning. The corresponding chromatographic profile is called breakthrough curve (BTCs), an example for one can be found in Figure 3. The basic scheme used in Figure 3 was taken from a publication by Nashaat[32] and modified by the thesis author to better suit the figure explanation.

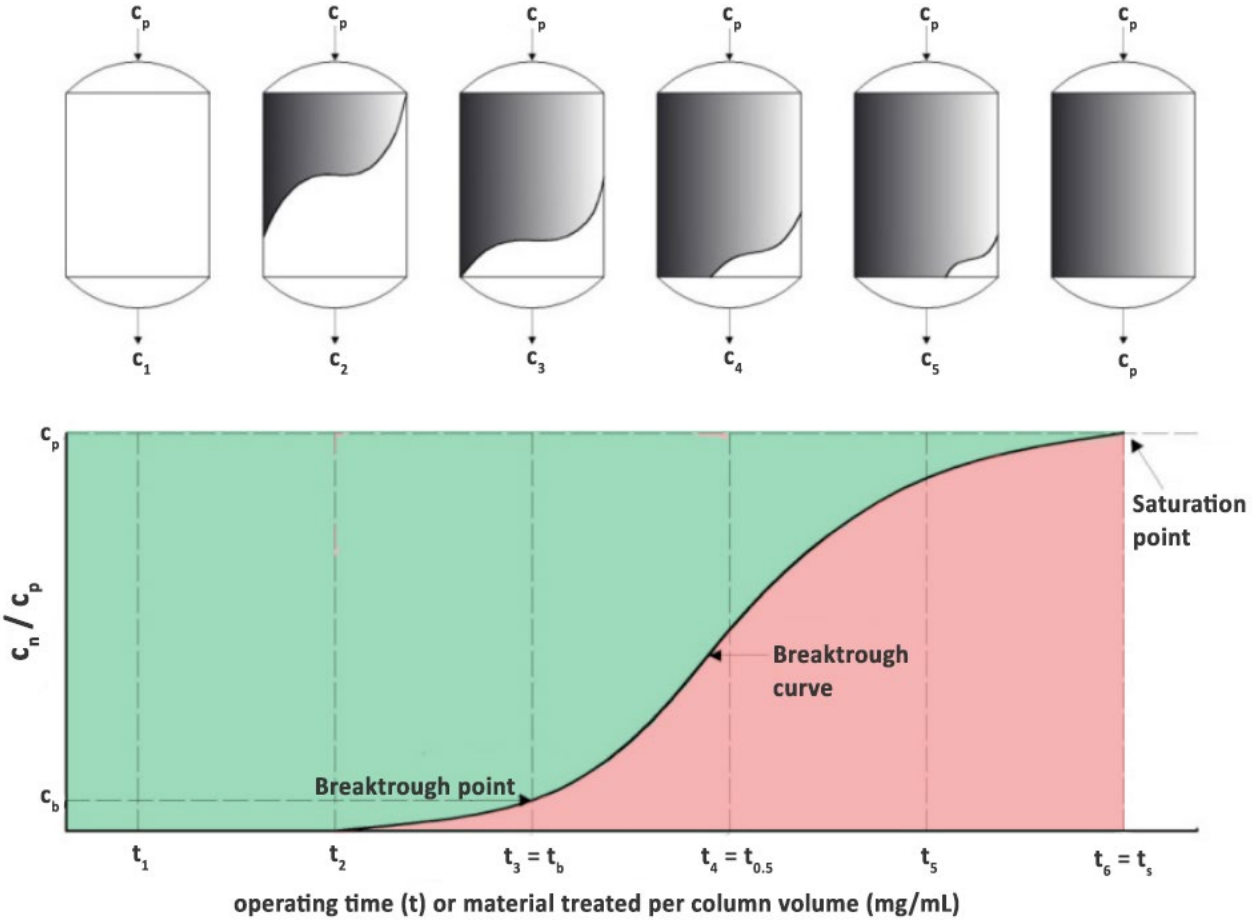

Figure 3: Graphical depicture of a breakthrough curve including column load trend. On the upper part of the Figure a column is loaded with bulk fluid with an initial concentration of c_p, the different loading states can be seen in the progress of protein adsorption onto the column, the fluid leaves the column with a concentration c_1 … c_n. On the lower part of the graph the corresponding breakthrough curve can be seen with timepoints t_1 … t_6, with t_b being the breakthrough time, t_s being defined as the saturation time, c_b as the breakthrough concentration

In a fixed bed column, a shock front wave through the bed is generated. This can be seen on the upper graph part of Figure 3. As implied in the graph this front usually does not move in a straight static way downwards. Effects like axial dispersion (mentioned in Section 2.3.2) or other hydrodynamic phenomena might contribute to an uneven front band width. The dark covered area in the column is known as mass transfer zone (MTZ). In the MTZ the sorption and desorption processes onto the stationary phase can be found. The green area in the lower part of Figure 3 represents the mass transfer zone while the red area depicts the fresh adsorbent zone in the fixed bed column adsorption process. The saturation point, when an equilibrium of inlet feed = outlet feed has been reached usually points out the end of the experiment. It is marked by $c_n = c_p$ in Figure 3, c_n/c_+ indicates the so-called operating limits of the column. The shape of these BTCs is influenced by the adsorption isotherm,

particle size and the different diffusion effects taking place during adsorption. Advantage of BTCs are that they can be carried out in small scale columns (< 1 mL columns) and the evaluated parameter used for upscaling at a later time point. Disadvantage would be the increased usage of protein and loading material that is required in the loading process.

An important parameter when examining BTCs is the dynamic binding capacity (DBC). It is defined as the capture efficiency at a specific breakthrough value. DBC are usually stated as 5% or 10% breakthrough, they can be found at a c_n / c_p of 0.05 or 0.1 in Figure 3.

3 Materials and Methods

3.1 Materials

Heat shocked, lyophilized BSA (bovine serum albumin) with purity of at least 98% was purchased from Sigma Aldrich (lot: A9647-100G).

3.1.1 Chromatography

CIP of columns was done using 0.1 M NaOH. All columns were stored in 20% Ethanol if not needed.

Table 1: List of columns used in the process of the thesis

CV (mL)	Resin	Mechanism
0.5[a]	Q Sepharose Fast Flow	AIEX
0.2[b]		
0.5[a]	Q Ceramic HyperD F	
0.2[b]		
0.5[a]	Fractogel EMD TMAE Hicap (M)	
0.2[b]		
0.2[b]	GigaCap Q-650M	
23.6[c]	Superdex 75	SEC
88.7[a]	Sephadex G25	
3078.8[a]	Superdex 75	

[a] columns were self-packed

[b] columns were purchased from Repligen Corporation

[c] column was purchased from Cytiva

Table 1 gives a summary over the columns and resins used during this thesis. An ÄKTA Explorer 100 system (including P-920 system pump, UPC-900 UV/VIS monitor modules as well as an 50 mL superloop) from Amersham Biosciences was used for the lab scale chromatography experiments. All pilot scale chromatography experiments were carried out using an ÄKTA Pilot system (including P-907 system pump, P-908 sample pump, UV-9010 UV/VIS monitor, bubble trap and air sensors) from GE Healthcare.

3.1.1.1 AIEX Chromatography

AIEX Buffer system composition was chosen according to Kelley et al.[33]

- Strong Binding Buffer: pH 8.1 (22 mM Tris HCl with no added NaCl)
- Strong Binding Elution Buffer: pH 8.1 (22 mM Tris HCl with 1 M NaCl)
- Weak Binding Buffer: pH 7.0 (50 mM HEPES with 65 mM NaCl)
- Weak Binding Elution Buffer: pH 7.0 (50 mM HEPES with 1 M NaCl)

AIEX resins used involved:

- Q Sepharose Fast Flow (Cytiva, average d_p = 9*10^{-3} cm
- Q Ceramic HyperD F (Pall Biosciences, average d_p = 5*10^{-3} cm)
- Fractogel EMD TMAE Hicap (M) (Merck Millipore, average d_p = 7.2*10^{-3} cm)
- TOYOPEARL GigaCap Q-650M (Tosoh Bioscience, average d_p = 7.5*10^{-3} cm)
- POROS 50 HQ (Applied Biosystems, average d_p = 5*10^{-3} cm)

Tricorn Packing Equipment 5/50 (Cytiva) was used for packing of the 0.5 mL columns. Solutions used for column packing involved 0.1 M NaCl, 0.4 M NaCl as well as 0.8 M NaCl

3.1.1.2 SEC Chromatography (buffer exchange)

Phosphate Buffered Saline (PBS) was implemented as SEC standard running buffer (if not mentioned otherwise). Preparation of 1L PBS was done as following:

- 0.137 M NaCl
- 0.0027 M KCl
- 0.01 M Na_2HPO_4
- 0.0018 M KH_2PO_4
- Adjust pH to 7.4

Buffer exchange SEC chromatography resins used involved:

- Sephadex G25 (Cytiva)

As an early used alternative PD-10 desalting columns (containing Sephadex G25 resin; Cytiva) were utilized in an effort for early buffer change experiments. Additional equipment involved:

- Omnifix F Luer Solo 0.01 – 1 mL (BRAUN)
- Millex-GV PVDF 0.22 µm (Merck Millipore)
- HiScale 26/200 empty column (Cytiva)
- AxiChrom 100-500 empty column (Cytiva)

3.1.1.3 Isotherm

- MiniSpin Benchtop Centrifuge (Eppendorf)

3.1.1.4 Batch Adsorption

- Omnifix F Luer Solo 0.01 – 1 mL (BRAUN)
- Millex-GV PVDF 0.22 µm (Merck Millipore)

3.1.2 Analytic

For total protein concentration measurement an UV/VIS Spectroscopy GENESYS 10S VIS (Thermo Scientific) was used. BSA protein samples were measured using a quartz cuvette (l = 1 cm) at 280 nm.

3.1.2.1 Analytical SEC

For analytical SEC, Phosphate Buffered Saline (PBS, composition see Section 3.1.1.2) was chosen as buffer system. The column used for the analytical SEC comprehends of a 10/300 (CV = 23.6) Superdex 75 (Cytiva) prep grade column. Additionally, the following equipment was used for proper sample injection:

- Omnifix F Luer Solo 0.01 – 1 mL (BRAUN)
- Millex-GV PVDF 0.22 µm (Merck Millipore)

3.1.3 Software

- CADET Web Interface (based on CADET Toolkit Version 3.0.0)
- SigmaPlot 13.0 (Systat Software Inc.)
- PeakFit Version 4 (AISN Software Inc.)
- TableCurve 2D v5.01.01 (Systat Software Inc.)
- Unicorn Version 5.11 (Build 407) (Cytiva)
- Office 365 Suite (Microsoft)

3.2 Methods

3.2.1 Chromatographic experiments

3.2.1.1 ÄKTA Pilot (monomer isolation)

An ÄKTA Pilot was used to separate BSA monomer in PBS from its multimers on a larger scale than possible on the ÄKTA Explorer 100. For this a 3078.8 mL column packed with Superdex 75 was used with an AxiChrom 100/500. The system equilibration block was done by using 30 mL of adequate buffer, column equilibration was set to 1 CV. The Bubble Trap was disabled for these runs. Overall run length of the monomer isolation was set to 0.5 CV. Flow for system and column equilibration as well as the sample load was set to 39 mL/min. The pressure difference maximum (ΔP) of the column was adjusted to 0.5 MPa. The UV/VIS baseline was monitored at 280 nm. Collection of BSA was programmed to set in at above and stop below 150 adsorption units (AU).

3.2.1.2 PD-10 desalting columns

First buffer change experiments were done by using PD-10 desalting columns from Cytiva Corporation. The columns were equilibrated using 15 mL of new buffer and applying 2.5 mL of sample gained during monomer isolation (see Section 3.2.1.1) onto the tubes after equilibration. Salt exchange procedure and elution process was forced by adding 3.5 mL of new buffer. The eluate contained protein with the new buffer of choice, usually a recovery of 70 – 90 % protein in the eluate is common. It must be noted that the eluted sample is diluted. In addition, the columns must never run completely dry at any given moment during buffer change or storage afterwards.

3.2.1.3 ÄKTA Explorer 100 (buffer change)

When larger quantities of BSA in weak or strong binding buffer were needed, a switch to a larger column containing Sephadex G25 resin (CV = 88.6 mL) was required. The resin was packed in an HiScale 26/200 column. The ÄKTA Explorer 100 system equilibration was set to 10 mL. The column equilibration was done using at least 1 CV of buffer. The sample was loaded using a 50 mL superloop, the run length was set to 1.5 CV to allow washout of later trending PBS. The Flow for system and column equilibration was set to 10 mL, sample load flow was set to 5 mL due to pressure constrains. The pressure maximum of column was set to 0.6 MPa, UV/VIS baseline was monitored at 280 nm. The collection of BSA was programmed to set in at above and stop below 150 Adsorption units.

3.2.1.4 Packing of 0.5 mL AIEX columns

The chromatographic column was packed by using 2 x CV as resin volume (e.g. 0.5mL of CV leads to the usage of 1mL of the stirred up resin) and washed up to 5 times with packing solution. The slurry is finally equilibrated as a 50 - 60% suspension. The packing solution consisted of either 0.1M NaCl or distilled water, according to the packing guideline manual provided by the manufacturer.

For the packing process the empty tricorn column was filled with the required amount of slurry. The tricorn adapter was placed and tightened on top of the column to allow a fitting of the adapter stamp with the solution. In order compress the slurry into a proper column package, the filled tricorn column was mounted into the ÄKTA Explorer 100 setup, and an adequate flow was started to allow a compact settling of the resin particles. The appropriate packing solution was used as mobile phase. This process must be done quite fast to avoid settling of the resin particles. If the particles settle to early the top adapter must be unscrewed and the particles in the slurry must be set into motion again to restart the packing process.

If the procedure was successful and the particles began to settle in, the flow can be raised to gain a proper package bed of the resin. After completing this step, the tricorn adapter was screwed firmly to close the whole column. Testing of the packed column asymmetry was done according to Section 3.2.2.1.

3.2.1.5 ÄKTA Explorer 100 (breakthrough curve)

For evaluation of the diffusional behavior, breakthrough experiments or also called frontal analysis experiments, were conducted. For this purpose, the column is overloaded with protein until a state of saturation is reached in the column. The unbound protein excess leaves the column and is recorded by the UV/VIS detection unit. The excess of protein that is needed to trigger this behavior is dependent on the resin, it can preliminary be estimated by performing adsorption isotherms.

For the system equilibration of the ÄKTA Explorer 100, 10 mL were used. AIEX columns were equilibrated with 2 times the CV. The initial flow for set to 2 mL/min, for the loading of the sample onto the column it was set according to the linear velocity *u* planned for the experiment. Maximum column pressure was set to 0.5 MPa. The UV/VIS baseline was monitored with the detection unit at 280 nm. The sample was loaded using a 50 mL superloop. During the breakthrough curve recording, excessive protein was recovered by collection. An automated collection of BSA was set in to start above and stop below 150 Adsorption units. After the breakthrough curve was recorded, the column was washed with 4 x CV running buffer. For the removal of bound protein, a step gradient was applied. The gradient buffer consisted of loading buffer + 1 M of NaCl. After the gradient, a CIP step with 4 times the CV of 0.1 M NaOH was performed. The Column equilibration step consisted of 4 x CV loading buffer. Resulting experimental UV/VIS data that was recorded during the run was normalized by setting it in ration versus the previously measured bypass adsorption of the protein feed.

3.2.1.6 Analytical SEC

For the analytical SEC analysis, a Superdex 75 prep grade 10/300 column was equilibrated using 1 CV of PBS. The chromatographic flow was adjusted to 0.5 mL/min, the column pressure alarm was set to 1.8 MPa. The UV/VIS baseline was monitored at 280 nm. 100 µL of sample were injected into the system with a proper sample loop, elution of the sample was also done by PBS. Run length was set to 1.5 CV to ensure washing out of all sample components.

3.2.1.7 Isotherm

The resin of choice was stored in 20% Ethanol solution and had to be washed up to 5 times with the buffer of interest. For this purpose, the resin was stirred up and a precalculated amount of slurry was taken. This slurry was centrifuged with a centrifuge for 5 min at 13.000 rpm. The supernatant was removed, and buffer was added. The amount of buffer is according to the amount of resin that is present. E.g., if 1 mL of resin is present another 1 mL of buffer must be added. This order of sequence is repeated up to 5 times, in the final washing step a ratio of 50% resin and 50% buffer is aimed for.

A pre-defined volume of slurry was added to a defined volume of protein of interest with determined concentration. This was done several times according to the planning of the isotherm experiment, varying the amount of slurry used each time. The mixture was equilibrated on an overhead rotating wheel for at least 24 hours. After incubation the samples were centrifuged for 30 min with 13.000 rpm, the supernatant was separated from the rest of the samples. The remaining, unbound protein concentration was measured with UV/VIS spectroscopy at 280 nm from Section 3.2.3.

Evaluation of the amount of protein bound to the resin after the experiment occurs according to Equation 3.1.

$$q_{bound} = \frac{\left(C_{protein} * V_{protein}\right) - \left(C_{protein\ supernatant} * \left(V_{protein} + V_{slurry}\right)\right)}{1 - \varepsilon} \qquad 3.1$$

Whereas $C_{protein}$ is the concentration of the protein used for the assay, $V_{protein}$ is the amount of protein used for the assay. $C_{protein\ supernatant}$ describes the concentration of the protein left in the supernatant after centrifugation and V_{slurry} gives the amount of slurry used in the conforming experiment. ε is the void fraction of the column and estimated with 0.35 for these experiments.

In addition, the corresponding Langmuir isotherm data for the experimental dataset is calculated according to Equation 2.2.

3.2.1.8 Batch Adsorption

As in Section 2.3.2.3, slurry containing 50% resin and 50% buffer of choice was prepared for the experiment. This washing, centrifugation and equilibration steps were done according to the resin washing part of Section 3.2.1.7. The slurry then was mixed with a protein solution of defined amount, the protein solution was setup with a magnetic stirrer at low speed to ensure proper mixing and avoiding the formation of air bubbles. At certain time intervals samples were drawn and filtrated using a syringe and the 0.22 µm sterile filter to stop the adsorption process. The remaining BSA concentration in the samples was later measured using the UV/VIS procedure from Section 3.2.3. Evaluation of the data was done by fitting the according pore diffusion model (Equation 2.37 to Equation 2.45) and surface diffusion model (Equation 2.46) to the experimental data .

3.2.2 Column and chromatographic data characterization

3.2.2.1 Asymmetry evaluation

The asymmetry of the packed columns was tested under non-binding condition by injection of a small 0.8 M NaCl aliquot onto a background of 0.4 M NaCl (pulse injection). Integration of Peaks was done using PeakFit, the asymmetry was calculated according to the so called Exponentially Modified Gaussian (EMG) function explained by Carta and Jungbauer in Chapter 8[4] of their book.

3.2.2.2 HETP evaluation

The HETP (height equivalent of a theoretical plate) were determined from frontal analysis experimental data. The data was loaded and fitted in TableCurve 2D, whereas a Savitzky-Golay smoothing with a win n of 20, 4 order, 3 passes and the 1st derivation was applied. A curve-fit peak equation with an exp-mod gaussian model and medium (Lorentzian) minimization was chosen to generate a fit. The model with 5 parameters (a, b, c, d, e) was selected and used for the determination of the first and second momentum according to Savoy[34] with Equation 2.7 and Equation 2.8.

3.2.2.3 Pore diffusion parameter evaluation

The determination of pore diffusion parameter was only possible for experimental data that could be fitted to the model. It was done according to Equation 2.23 – Equation 2.28 by calculating data from the pore diffusion model using the constant pattern solution of Weber et al.[26].. Further details of the referenced model include void fraction *ε,* which was assumed as 0.35, as well as q_m which is defined as amount of solute adsorbed per unit particle volume (mg protein/ cm³ particle) in the mathematical model. However, for the graphical solution of the model, q_m is described as amount of solute adsorbed per unit resin volume (mg protein / ml CV) in the corresponding graphs. These propositions are also valid for Section 3.2.2.4.

3.2.2.4 Surface diffusion parameter evaluation

An analytical solution of the packed bed equation from Section 2.3.2.2.2 was used to generate an according surface diffusion model for the experimental data. It uses the lower curve from Equation 2.29 and the upper curve calculation from Equation 2.30 with the corresponding conditions. The model boundary conditions and assumptions mentioned in Section 3.2.2.3 are also valid for this model.

3.2.2.5 Parallel diffusion parameter evaluation

For evaluation of the parallel diffusion model parameter CADET Web (https://www.cadet-web.de) is used. It offers a browser-based GUI to the CADET framework and consists of the CADET solver version 3.0.0 that is powered by Python 2.7. The web interface uses a PostgreSQL database for server-side data storage. CADET software offers a fast and accurate solver for the general rate model (see Section 2.3.2) of packed bed liquid-chromatographic systems. For more information onto CADET see the handbook created by von Lieres and Leweke[35].

The CADET Web interface allows the creation and run of single and multiple set up of experiments at once including live comparison of multiple datasets. The calculated experiments can be stored online for later usage. CADET Web requires all input units to be in SI unit format, which means that data using other conventional units must be converted to the SI unit format first.

The general parameters that were used for each simulation are defined and entered according to the following narration. To start the simulation a new simulation was created, and the normal user interface mode was used. In the first tab, the number of components was set to 1, the number of steps to 1 and the type of Isotherm was set to the multi component Langmuir model. For the column setup tab, a column porosity of 0.30, a particle porosity of 0.72 for Q Sepharose Fast and 0.71 for Fractogel EMD TMAE Hicap(M) resin was used. These values were determined by CADET simulation experiments. A column dispersion of $7.2*10^{-8}$ m²/s was calculated as to Section 4.6.3, the mobile initial concentration and bound initial concentration was set to 0. In the Isotherm setup tab, the isotherm binding model was chosen and a K_D of 1 was entered. The loading setup tab consists of 2 sub-tabs, in the first times sub-tab the start step 1 was set to 0 s, the end step was set to 3000 s. The second step 1 subtab describes component 1 in detail, a constant of $3.1 *10^{-2}$ mol/m³ was chosen with a linear of 0 for the only component of the simulation. In the discretization tab a column discretization of 50 and a particle discretization of 5 was used. All other turning up windows and tabs were accepted, and the simulation was started. Any parameters that differ from this listing or are missing were used according to Section 4.6. The output of the simulations is downloaded as an .xlsx dataset, converted into conventional units and imported to the already existing corresponding experimental chromatographic dataset for the purpose of comparison.

3.2.3 BSA photometer measurement

Concentration of proteins was calculated using Lambert-Beer law:

$$A = c\ \varepsilon_A\ l_c \qquad 3.2$$

Where A is the absorbance, ε_A is the molar absorption coefficient (0.667 L $M^{-1}cm^{-1}$ for BSA), c is the molar concentration of interest and l_c is the path length of the quartz cuvette (1 cm). BSA was measured at 280 nm. Blank was set by using 1 mL of adequate buffer, sample was diluted properly up to 1 mL into the range of the UV/VIS concentration law (0.2 – 0.8).

4 Results and Discussion

4.1 Preparation of BSA samples

For isolation of the BSA monomer, 10 g of crude, heat shocked fraction BSA were dissolved at room temperature in approximately 333 mL of PBS (30 g/L). 100 mL of this solution were loaded onto a Superdex 75 100/392 column (CV = 3078.8 mL, see Section 3.2.1.1).

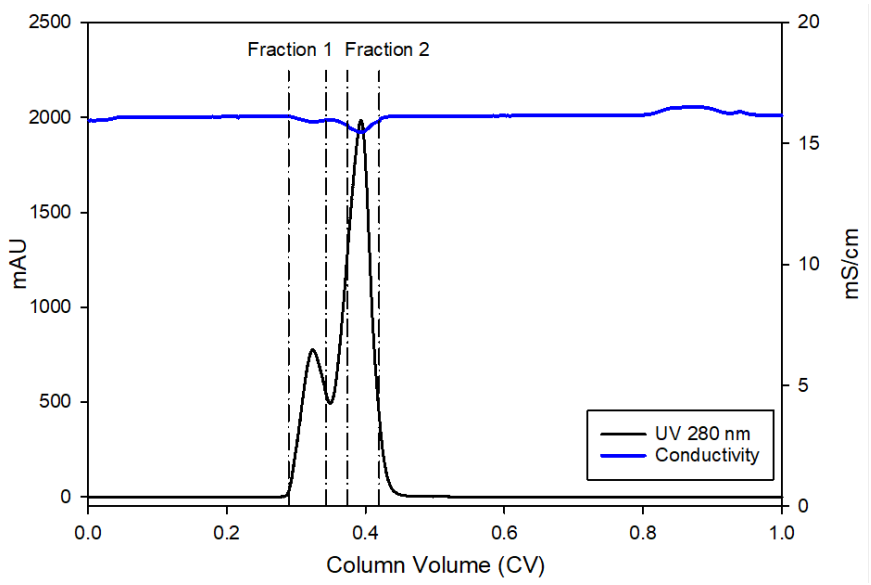

Figure 4: Separation of crude BSA in PBS on a Sephadex G25 100/392. Fraction 1 peak indicates the multimer, Fraction 2 peak represents the monomer. 100 mL of the sample were injected onto an ÄKTA pilot with a linear velocity of 31 cm/h.

Figure 4 indicates the monomer to multimer separation of these crude BSA samples, fraction 1 (multimer) and fraction 2 (monomer) were collected. The start of fraction 2 collection was intentional set late to ensure a cut-off on the overlapping BSA multimer. Monomer fraction 2 was used further on, multimer fraction 1 was stored at 4°C if needed.

Figure 5 shows the monomer content of fraction 2. It was checked by an analytical SEC on a Superdex 75 10/300 (CV = 23.6 mL; see Section 3.2.1.6) with 50 µL of undiluted sample. To ensure the integrity of this sample a comparison with a column performance control dataset, provided by the column supplier Cytiva, was drawn[36]. They presented a molecular size marker dataset containing (a) bovine serum albumin (67 kDa, 8 mg/mL); (b) ovalbumin (43 kDa, 2.5 mg/mL); (c) ribonuclease A (13.7 kDa, 5 mg/mL); (d) aprotinin (6.512 kDa, 2 mg/mL); and (e) vitamin B12 (1.355 kDa, 0.1 mg/mL). 500 µL of this mix was injected with a flow rate of 0.4 mL/min using a 0.05 M phosphate buffer with 0.15 M NaCl and pH 7.0 at room temperature by them and detected at 280 nm. The peaks of Fraction 2 monomer BSA and the one provided by the supplier (a) did match.

In total 3 runs were carried out by using the prepared BSA solution. Fraction 2 (monomer fraction) of all runs was applied to an analytical SEC for a monomer examination and pooled afterwards if enough purified monomer material was present.

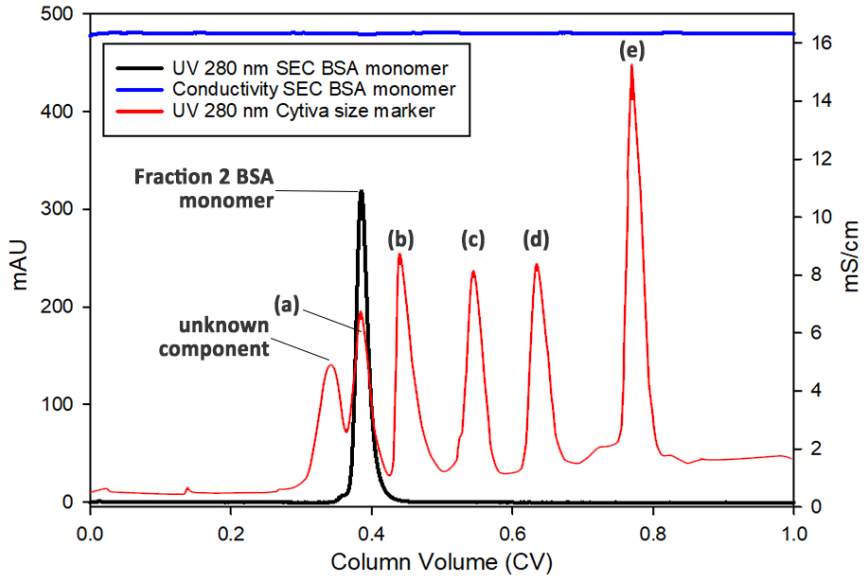

Figure 5: Analytical SEC Evaluation of an undiluted BSA Fraction 2 sample from Figure 4 in comparison to a molecular size marker mix dataset provided by the supplier. 50 µL sample were injected undiluted onto a Superdex 75 10/300 column. It was analyzed on an ÄKTA Explorer 100 with a linear velocity of 38 cm/h due to pressure constrains. The peak identity profile proves the affiliation of the fractionized BSA monomer, and a dataset provided by the supplier. First peak on the red molecular size marker chromatogram, represents a substance than cannot be identified, (a) is BSA monomer, (b) to (e) represent the other components.

Initially, PD-10 desalting columns (see Section 3.2.1.2) containing Sephadex G25 SEC resin were used to rebuffer the PBS of BSA monomer fraction to strong or weak binding buffer of choice (for strong / weak binding buffer composition see Section 3.1.1.1). However, this method only allowed the generation of limited amount of sample with a low productivity. In the following, a more efficient way of rebuffering was introduced to generate material for the upcoming experiments.

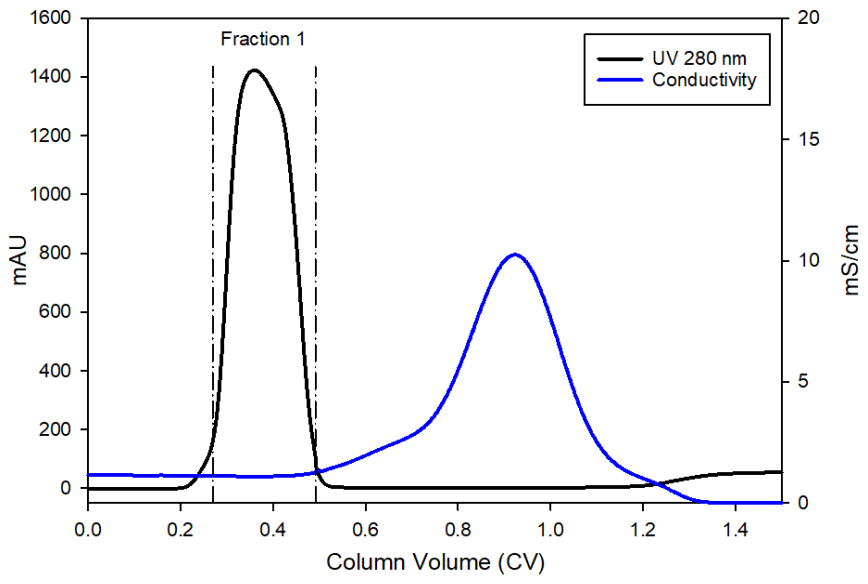

Figure 6: Buffer exchange of BSA monomer from PBS to strong binding buffer on a Sephadex G25 26/167. Injection material for this buffer change was Fraction 2 from Figure 4. The sample was injected onto an ÄKTA Explorer 100 with a linear velocity of 57 cm/h. Fraction 1 peak indicates BSA with strong binding buffer while the conductivity peak represents the later eluting PBS.

An HiScale 26/200 column was packed with Sephadex G25 resin (CV = 88.7 mL) and further on used in the process of rebuffering to generate adequate amount of recently prepared BSA binding buffer

sample (see Section 3.2.1.3). Prior to the isotherm determination, protein sample was exchanged into the respective binding buffer using the gel filtration method mentioned in Figure 6. It shows the chromatographic profile of a buffer exchange, the initial conductivity of the strong binding buffer (1.1 mS/cm) started to shift upwards as PBS eluted (up to 10 mS/cm), which was later excluded from the column than the initial strong binding buffer. Fraction 1 sample was therefore eluted with strong binding buffer (lower overall conductivity).

The usage of freshly prepared sample stocks was necessary since the monomers degraded over time. SEC and photometric analysis proved that there was a significant decrease in the amount of available BSA in the samples.

4.2 Adsorption isotherms

Initially implemented resin strategy involved different microporous and polymer-grafted anion exchangers

- Cross-linked agarose beads (Q Sepharose Fast Flow, average $d_p = 9*10^{-3}$ cm)
- Polymeric polystyrenedivinylbenzene particles (POROS 50 HQ, average $d_p = 5*10^{-3}$ cm)
- Rigid ceramic sorbents (Q Ceramic HyperD F, average $d_p = 5*10^{-3}$ cm)
- Tentacle type graft resin (Fractogel EMD TMAE Hicap (M), average $d_p = 7.2*10^{-3}$ cm).

As mentioned in Section 2.2, the resins were assigned into two categories – macroporous and composite. Q Sepharose Fast Flow and POROS 50 HQ were assigned to the macroporous matrices, which are known for their structure of widely open and accessible pores. Q Ceramic HyperD F as well as Fractogel EMD TMAE Hicap (M) on the other hand do belong to the composite resins. Q Hyper D F can be described as gel-in-a shell media, Fractogel EMD TMAE Hicap (M) belongs to the sub-category of polymer grafted resins. All these resins mentioned provide immobilized anion exchange surface ligands for different interactions with the sample concerning ionic bonding, hydrophobicity and affinity.

The resins were chosen according to Zhang et al.[3], who already investigated the effect of the strong and weak binding buffer condition effects onto purified monomers of two mABs A + B, dimer of mAbB as well as multimer of mAbA. mAbA represented an IG2 antibody with a pI of 7.6, while mAbB represented an IG1 antibody with a pI of 8.6. They also partly investigated the effect of these buffer systems with BSA. In addition, Q Ceramic HyperD F with an average $d_p = 5*10^{-3}$ cm was added to the selection of resins in this work.

To generate more fundamental information on protein equilibria behavior for these resins in combination with the different buffer compositions, adsorption isotherm experiments were set up. They were important for determining the total binding capacity as well as the binding strength of BSA with the resin. The determination of these parameters also helped to estimate the amount of protein load that is going to be used in the frontal analysis experiments. In addition, the binding parameters were also used in the calculations of the parallel diffusion parameter of Section 4.6.3.

Figure 7 shows the adsorption isotherms for BSA on all resins that were used in the comprehensive testing of 0.5 ml AIEX columns. The graph also takes the two different binding buffers of the breakthrough experiments into account. All isotherms reached equilibrium state after 24h of incubation. Filled circles and filled triangles are experimental data while the crossing line is a fit of the Langmuir isotherm that was calculated according to Equation 2.2. The aim was to evaluate the fitted values of the binding capacity q_m as well as the adsorption constant K. These were determined by solving the fitted parameters against the non-linear minimized residual sum of squares using the implemented solver of Microsoft Excel.

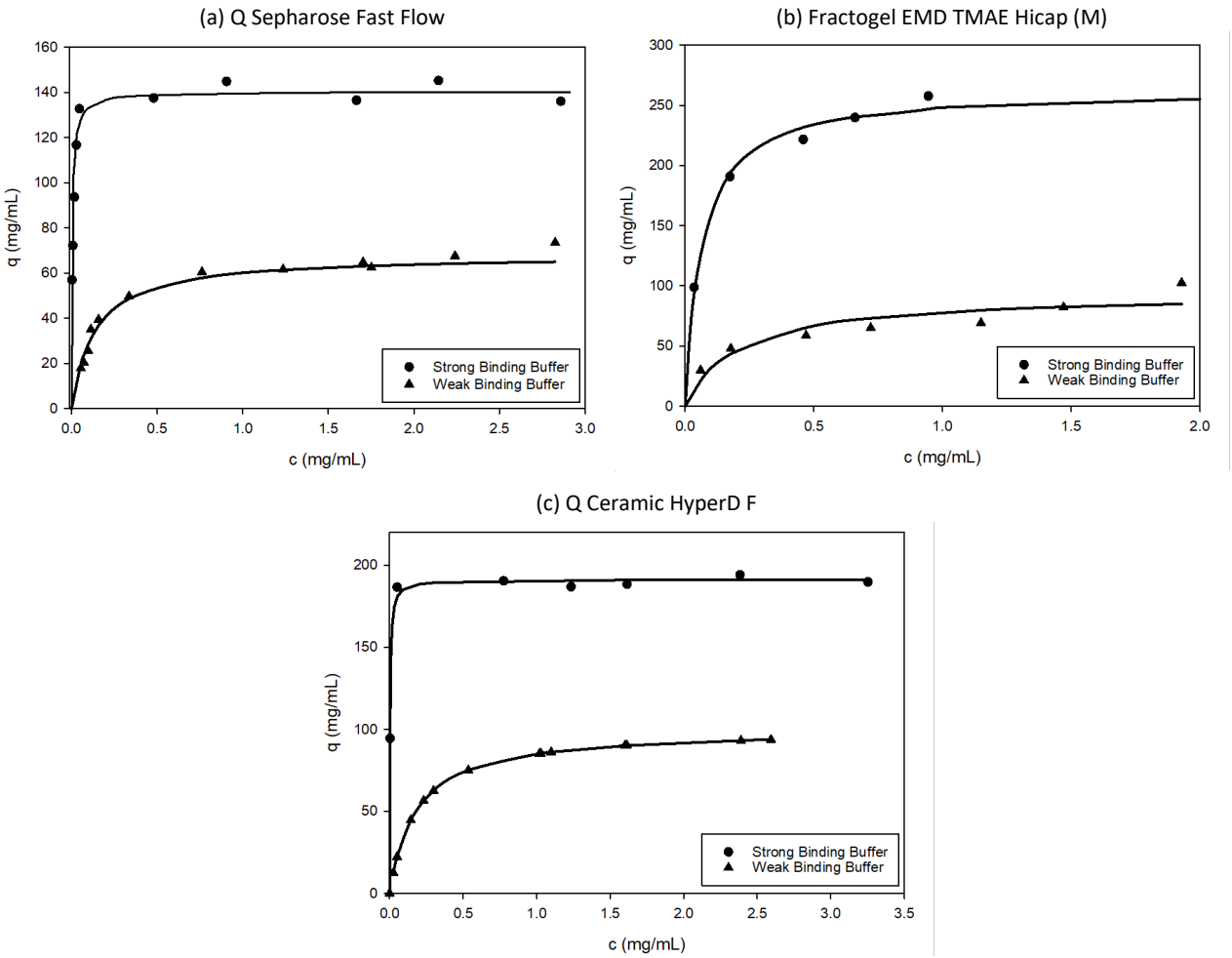

Figure 7: Adsorption Isotherms for chosen AIEX resins with corresponding Langmuir fit. Filled circles and triangles are experimental data while the crossing line represents the equivalent Langmuir fit. Adsorption isotherms were done for the strong binding buffer and weak binding buffer.

All weak binding buffer offered a significant decrease in protein binding capacity in comparison to their strong binding buffer counterparts as proposed by Kelley and coworkers[33]. Furthermore, BSA adsorption seemed highly favorable for all used stationary phases as well as the strong and weak buffer systems. According to the graphic output of Figure 7 all strong binding buffer isotherms can be assumed as rectangular. Weak binding buffer adsorption isotherms proposed an approximation to the rectangular model when using higher concentrations of protein.

Table 2 compares the binding capacity q_m of the adsorption isotherm experiments with available published data. The data it is compared to, can be found in brackets right next to it. Published data was only available in graphical form, therefore these values are estimated. Zhang et al. [3] used the exact same strong and weak binding buffer composition as was used in this thesis in combination for Fractogel and Q Sepharose Fast Flow resins. Therefore, the experiment, thus the results were comparable. Fernandez et al.[37] used 50 mM TRIS-HCl at pH 8.6 with the Q HyperD F resin, therefore results were quite comparable to strong binding buffer conditions. The used strong binding buffer consisted of 22 mM TRIS-HCl, no added NaCl and pH 8.1. However, weak binding buffer (50 mM HEPES, 65 mM NaCl, pH 7.0) adsorption isotherm results of Q HyperD F was compared to available Fernandez data with caution. The Buffer composition, especially NaCl concentrations differed, thus not comparable. Still, they are mentioned in Table 2 for sake of completeness. Also the Q Ceramic HyperD F composition used by Fernandez has changed over the timespan since the data was published in 1995. The current available Q Ceramic HyperD F particles are based on rigid ceramic beads while the resin

composition of 1995 Q HyperD F was based on composite porous silica-polyacrylamide. Thus, the physical properties of the particle have changed as the binding engagement of the particle has shifted interaction with the protein target. This of course changes the physical properties of the particle as it influences the particles binding engagement with its protein target.

Table 2 also gives an overview of the binding strength equilibrium constants that were calculated for the fits. No published supplemental data, that fits this experimental setup, was found to compare the experimental data to.

Table 2: Comparison of adsorption isotherm results that were experimental determined. The binding capacity q_m and Equilibrium constant K are in comparison to available published data. Adsorption isotherms were done for the strong binding buffer and weak binding buffer. Values in brackets are literature data for comparison.

Resin	**Strong binding buffer q_m (mg/ cm³particle)**	**Strong binding buffer K (mL/mg)**	**Weak binding buffer q_m (mg/cm³ particle)**	**Weak binding buffer K (mL/mg)**
Fractogel EMD TMAE Hicap (M)	263 (250 [3])	16.1	94 (100 [3])	4.8
Q Ceramic HyperD F	191 (220 [37])	333.6	100 (120 [37])	5.6
Q Sepharose Fast Flow	140 (135 [3])	182.5	68 (70 [3])	7.4

4.3 Packing and testing of 0.5 mL AIEX columns

4.3.1 Packing, performance testing and which columns to further use on

All 0.5 mL columns were packed as described in Section 3.2.1.4. The aim was to get a column height of ~20 mm. The column asymmetry testing of the columns was done using a salt pulse injection (see Section 3.2.2.1). A column overloading test was performed by doing a breakthrough experiment using 2 mg/mL of BSA in combination with weak binding buffer conditions on the packed column (see Section 3.2.1.5). The column overloading test served to exam if the column behaves as expected during the breakthrough conditions or if irregularities that are based on an insufficient package appeared. The linear velocity u for these frontal analysis experiments was set to 130 cm/h. In 0.5 mL columns this resulted in an effective residence time of 60 seconds. The film mass transfer coefficients k_f of the different resins were calculated according to Equation 2.12 with a linear velocity u of 130 cm/h, the appropriate resin particle diameter d_p, a kinematic viscosity v of 0.01 cm²/s, a free diffusivity D_0 of $6.77*10^{-7}$ (calculated in Section 4.6.3.1) and a column void fraction ε of 0.35. This resulted in the following film mass transfer coefficients:

- k_f (Q Sepharose Fast Flow) = $6.5*10^{-4}$ cm/s
- k_f (Q Ceramic HyperD F) = $8.7*10^{-4}$ cm/s
- k_f (POROS 50 HQ) = $8.7*10^{-4}$ cm/s
- k_f (Fractogel EMD TMAE Hicap (M)) = $7.2*10^{-4}$ cm/s

The results of this frontal analysis overloading tests are displayed in Figure 8. The Poros50 resin was discarded from the resin strategy list after several tries since none of the packed columns successfully passed the corresponding overloading test. All other columns mentioned in Figure 8 passed and were used further on during the frontal analysis experiments.

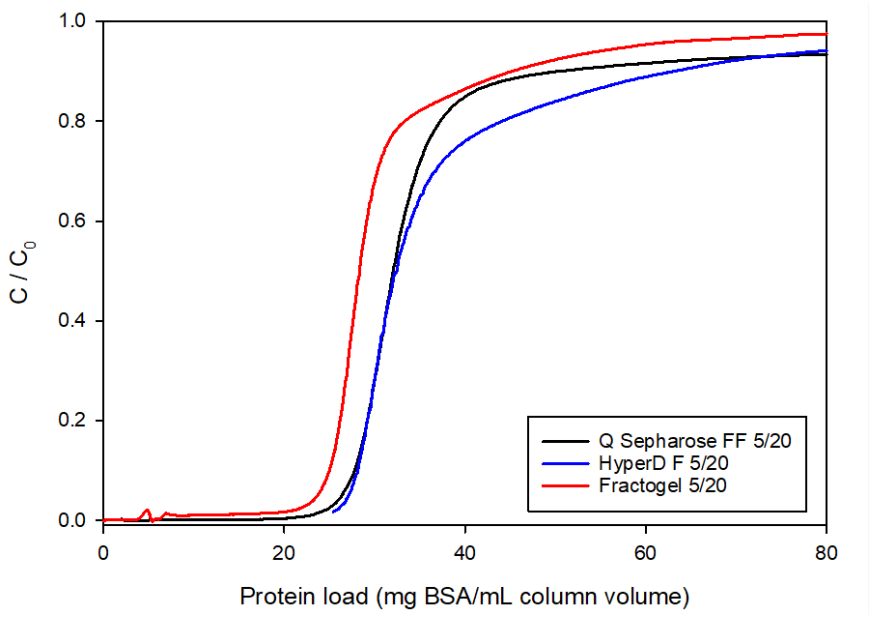

Figure 8: Comparison of 0.5 mL column breakthrough curve overloading test results. Only columns that passed the overloading test are displayed. The experiments were done on an ÄKTA Explorer 100 with weak binding buffer conditions, a linear velocity of 130 cm/h and a BSA concentration of 2 mg/mL. The different curves represent the different resins used in the process of the breakthrough curves.

4.3.2 Comprehensive testing of 0.5 mL AIEX columns under different conditions

Since testing of packed columns from Figure 8 under weak binding buffer with 2 mg/mL BSA as requirement were successful, more conditions for the breakthrough curve experiments were applied to the columns. This served as a test to explain the differences of triggered mass transfer effects on each resin that were caused by changing conditions. Various authors[27; 38-40] gave strategies on how mass transfer rate and adsorption mechanism were influenced with varying protein concentration and different ion binding strength on ion-exchangers. Taking these studies into account, the following conditions were determined and going to be applied in the experiments:

- Linear velocity *u* of 130 cm/h (this resulted in an effective residence time of 60)
- Strong and weak binding buffer (see Section 3.1.1.1 for composition of buffer)
- 2 mg/mL and 0.2 mg/mL monomer BSA concentration
- 5/20 packed columns with chosen AIEX resins from Section 4.3.1
    - Q Sepharose Fast Flow
    - Q Ceramic HyperD F
    - Fractogel EMD TMAE Hicap (M)

Figure 9 and Figure 10 represent the results of the frontal analysis experiments under the chosen conditions. Figure 9a – b and Figure 10 a – b focuses on displaying all used resins in a graph while varying the protein concentration over the two pictures. Figure 9c – e and Figure 10c - e compares the two different protein concentration for the individual resins. Strong binding buffer was used as the corresponding buffer system for all experiments in Figure 9, Figure 10 displays the weak binding buffer results.

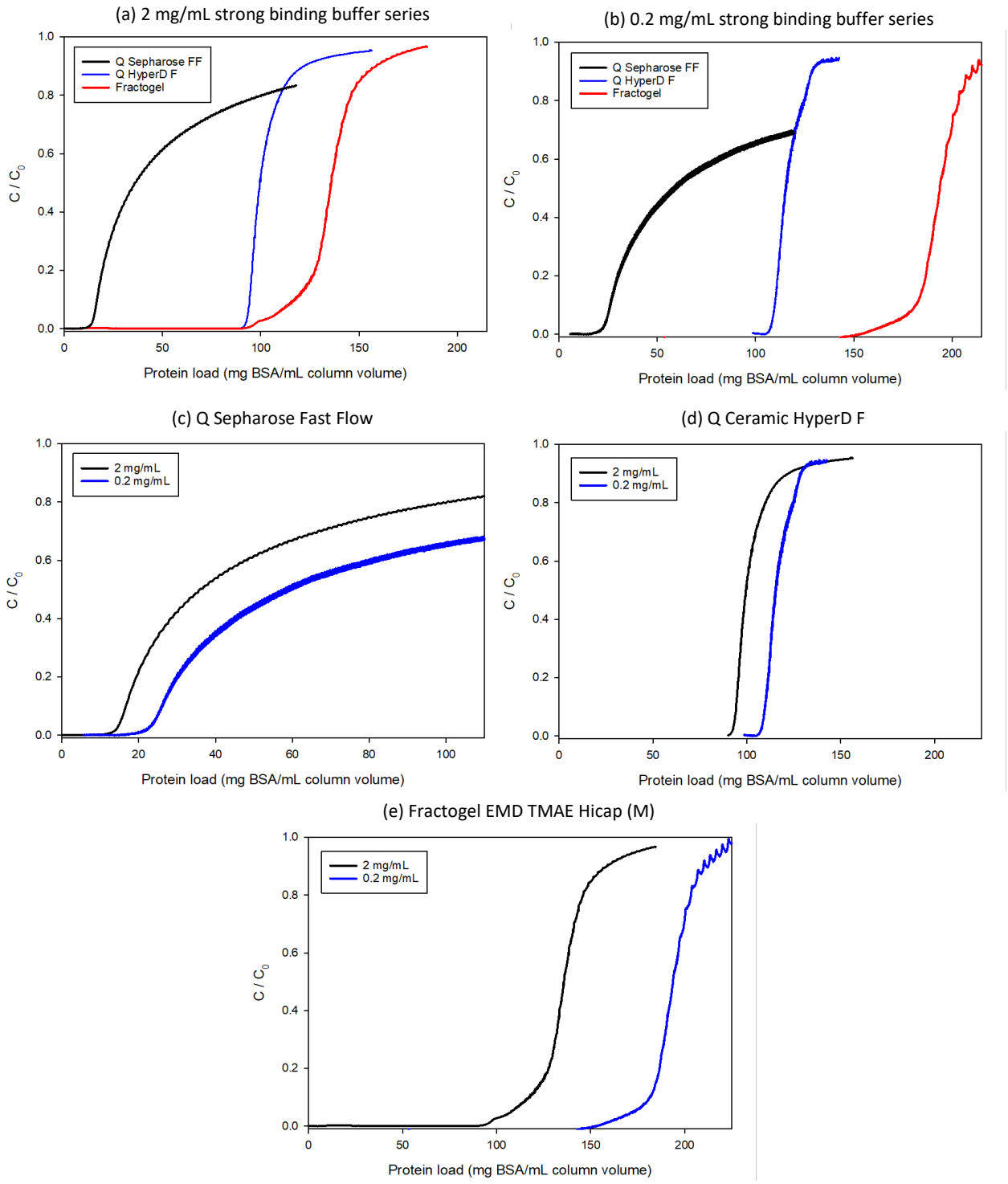

Figure 9: Results of strong binding buffer breakthrough curve experiments with selected 0.5 mL columns. The experiments were carried out on an ÄKTA Explorer 100 with a linear velocity of 130 cm/h, the BSA concentration was set to 2 mg/mL and 0.2 mg/mL. a – b compares the different resins with the same the protein concentration on different columns. c – d varies the concentration of the protein on the same resins.

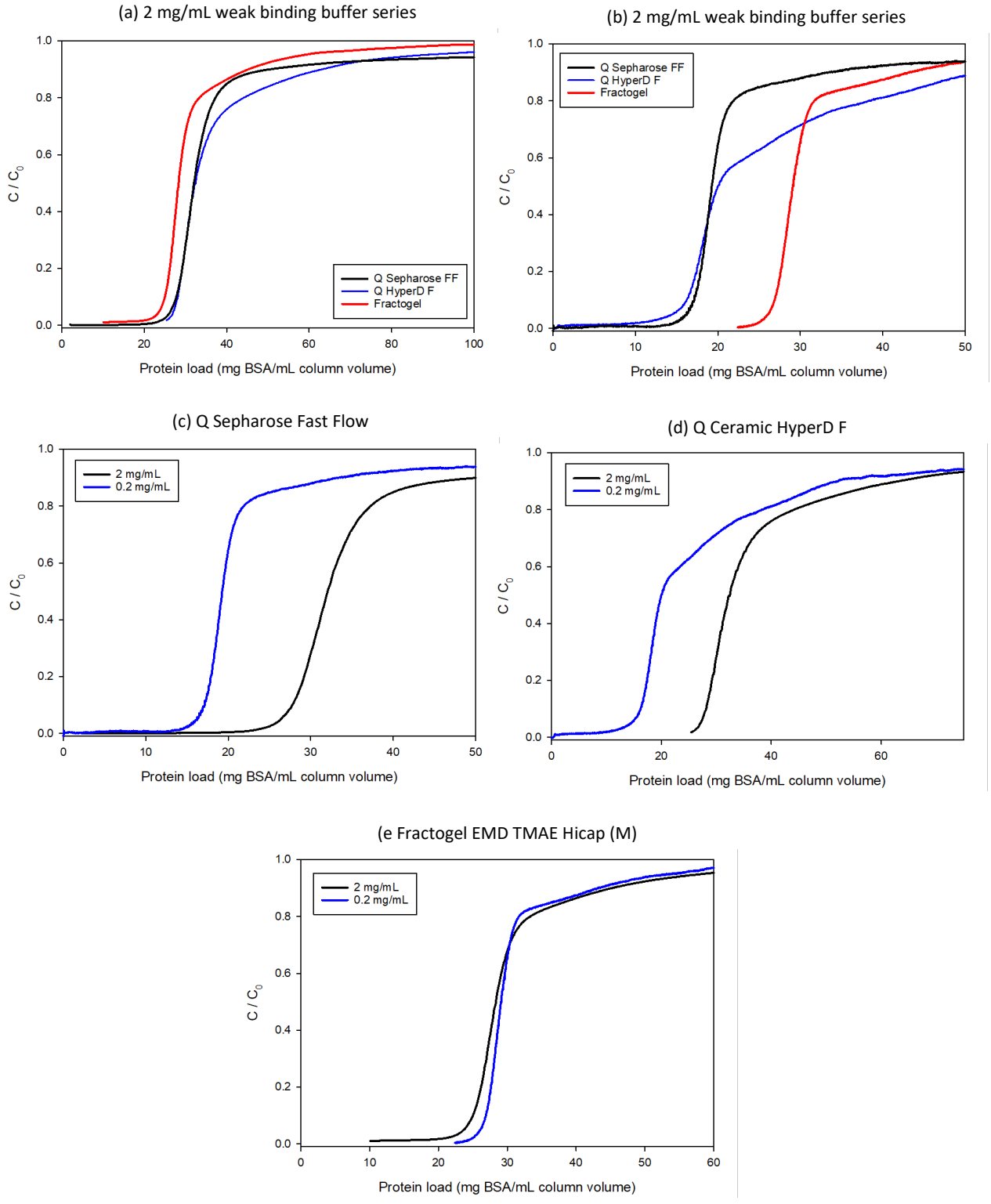

Figure 10: Results of weak binding buffer breakthrough curve experiments with selected 0.5 mL columns. The experiments were carried out on an ÄKTA Explorer 100 with a linear velocity of 130 cm/h, the BSA concentration was set to 2 mg/mL and 0.2 mg/mL. a – b compares the different resins with the same the protein concentration on different columns. c – d varies the concentration of the protein on the same resins.

The experimental results highlight that the baseline of the breakthrough curves suffered from the comparatively long runs. An example for this were the 0.2 mg/mL runs, especially Figure 9e, where the 0.2 mg/mL run showed heavy baseline fluctuation at the end of the frontal analysis experiments. Since a single 0.2 mg/mL run lasted up to 17.5h due to the slow sample loading, there needed to be an improvement. The overall run time of these experiments needed to be reduced, a possible solution for this was to minimize the bed volume of the column. This therefore resulted in smaller columns. In addition, the linear velocity *u* of the runs was increased, which resulted in much shortened chromatographic runs. This however imposed the risk of an worsened chromatographic performance if the columns could not properly handle the increased flowrate.

Another conclusion that was drawn from previously conducted experiments is the insufficient chromatographic column performance. The packing on some of the self-packed columns was insufficient and caused irregular flow uniformity which resulted in an early breakthrough of the curve. An example for an early breakthrough can be observed in Figure 9e (2 mg/mL and 0.2 mg/mL) and Figure 10d (0.2 mg/mL). The early breakthrough effect that happened on short scale columns (1-5 cm) has been described by Roberts et al. [41]

As the self-packed columns did not provide sufficient performance for this application, it was decided to conduct the following breakthrough curve experiments with commercially available pre-packed columns purchased from Repligen Corporation.

4.4 Batch adsorption

To further investigate the kinetics of the diffusion effects, batch adsorption experiments were done. The batch adsorption experiments were concluded according to the workflow mentioned in Section 3.1.1.4 for a protein concentration of 2 mg/mL. This was done for Fractogel EMD TMAE Hicap (M), Q Ceramic HyperD F and Q Sepharose Fast Flow resins with a protein concentration of 2 mg/mL. In addition, Toyopearl GigaCap Q-650M from Tosoh Bioscience was added to the list of resins, as it was another representative for the polymer functionalized media resins. This was done since Fractogel media already gave promising results in 0.5 mL column testing from Section 4.3.2 and to further research the indicated interphase parallel diffusion transport mechanism suggested in certain literature.[6; 42] The resin offers a structure similar to the Fractogel resin while providing a core of hydroxylated polymethacrylate beads that contain a grafted, novel bonded channel like phase structure with a particle size average of 75 µm.

The models for the kinetic data was calculated according to Equation 2.37 to 2.45 in Section 2.3.2.3.1 for the corresponding pore diffusion parameter and Equation 2.46 in Section 2.3.2.3.2 for the surface diffusion parameter. A film mass transfer coefficient k_f of $1.5*10^{-3}$ was assumed for the model evaluation. The numeric fitting results of these experiments are displayed in Table 3. The binding capacity of the weak and strong binding buffer experiments was comparable to the data that was determined by adsorption isotherms experiments in Table 2 of Section 4.2.

Table 3: Comparison of strong and weak binding buffer batch adsorption results that were experimental determined. The binding capacity q_m, pore diffusion coefficient D_e and surface diffusion coefficient D_s were evaluated by fitting the appropriate model to the experimental data.

	Strong binding buffer			**Weak binding buffer**		
Resin	**Binding capacity (mg/ cm³particle)**	**Pore diffusion coefficient (cm²/s)**	**Surface diffusion coefficient (cm²/s)**	**Binding capacity (mg/ cm³particle)**	**Pore diffusion coefficient (cm²/s)**	**Surface diffusion coefficient (cm²/s)**
Fractogel EMD TMAE Hicap (M)	183	$2.5*10^{-7}$	$2.5*10^{-9}$	75	$3.0*10^{-7}$	$1.0*10^{-8}$
Q Ceramic HyperD F	210	$2.0*10^{-7}$	$1.5*10^{-9}$	87	$1.5*10^{-7}$	$4.0*10^{-9}$
Q Sepharose Fast Flow	89	$4.0*10^{-8}$	$1.3*10^{-9}$	65	$2.0*10^{-7}$	$1.0*10^{-8}$
Toyopearl GigaCap Q650M	239	$2.0*10^{-7}$	$2.5*10^{-9}$	124	$3.0*10^{-7}$	$1.0*10^{-8}$

As can be seen in Table 3 all pore diffusion coefficients for the strong binding buffer series, except Q Sepharose Fast Flow, are in the approximately same range. The value for the Q Sepharose Fast Flow pore diffusion coefficient differed by a margin of 10 from the others, indicating a much slower possible mass transfer on that buffer system due to a reduced availability of pores. This behavior was not replicated on the surface diffusion model. For the weak binding buffer, Table 3 showed that all determined values were in the range of $1.5*10^{-7}$ cm²/s to $3.0*10^{-7}$ cm²/s. When fitting with the surface diffusion model it was noticed that Q Ceramic HyperD F showed a slightly reduced value in comparison to the other surface diffusion coefficients.

The protein adsorption in batch mode for a given time range of up to 90 minutes can be seen in Figure 11. In Figure 11a, b and c (Strong buffer series) the experimental curves (black dots) seemed to gain a state of transition that was not well captured by the models. This made it rather difficult to fit.

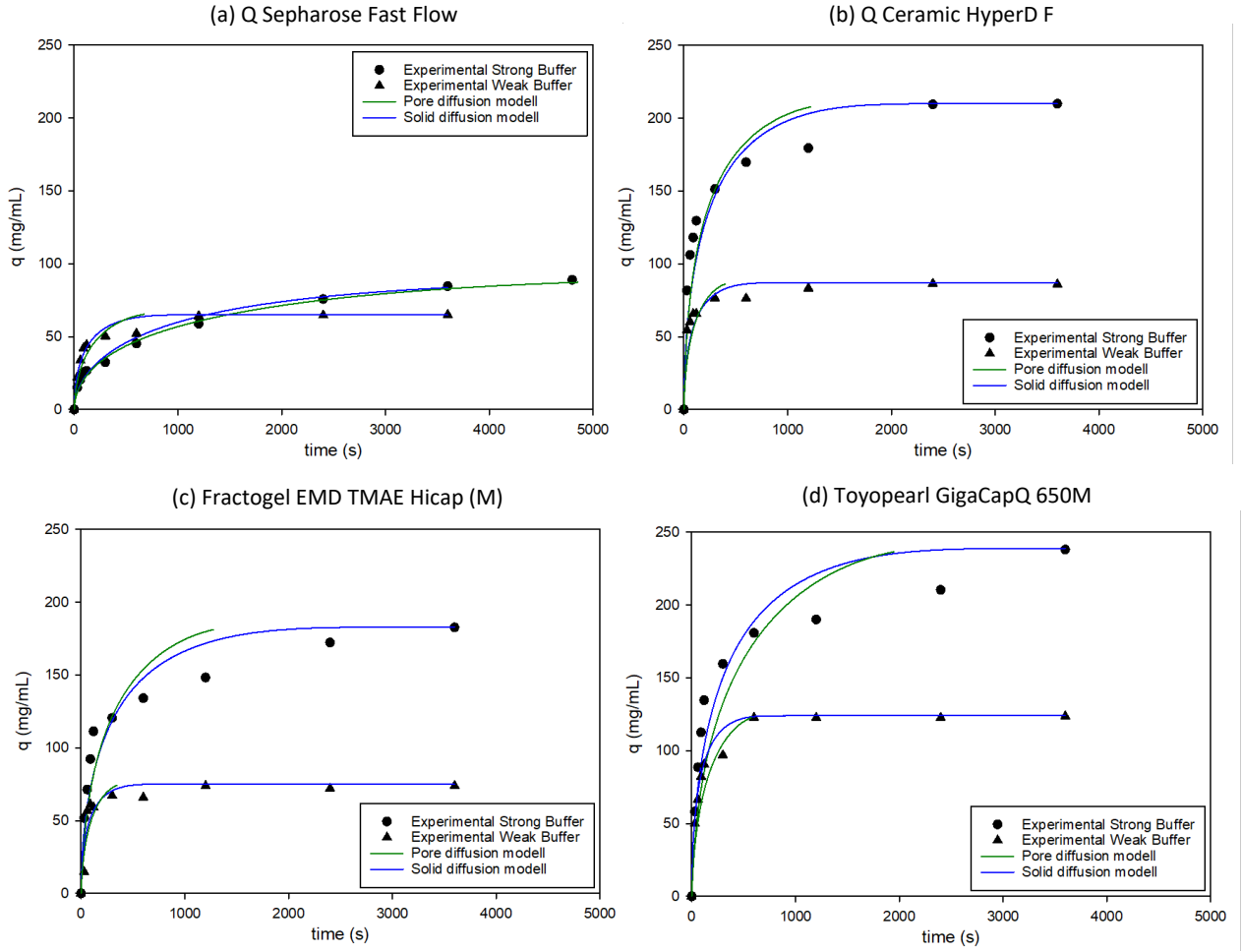

Figure 11: Batch adsorption for chosen AIEX resins with corresponding pore and surface diffusion model fit. Filled circles depict the strong buffer experiments while triangles are weak buffer experimental data. The colored, crossing lines represents the equivalent pore or surface diffusion model fit.

4.5 Experimental trials of 0.2 mL AIEX columns

As mentioned in the remarks of Section 4.3.2, a switch to commercially available columns was done to increase the chromatographic performance as well as to decrease the run time of the breakthrough experiments. This column change allowed the generation of additional data, while also lowering the amount of BSA used on each chromatographic run. The 0.2 mL columns (5 mm diameter, 10 mm length) were bought from Repligen Corporation. To prove replicability with the results generated on 0.5 mL columns and to scout possible differences in advance all 2 mg/mL experimental breakthrough curves from Section 4.3.2 were repeated.

The 0.2 mg/mL runs with a linear velocity of 130 cm/h were cut from the list of experimental approaches as they took too much time. The cancelled runs were instead replaced by 0.2 mg/mL runs with a linear velocity of 1000 cm/h, addressing one of the core problems mentioned in the remarks of Section 4.3. It was not possible to run 0.2 mg/mL 130 cm/h curves without any problems as the UPC-900 UV/VIS monitor module of the ÄKTA Explorer 100 FPLC system couldn't handle these long runs accordingly. Therefore, the focus was put onto a different linear velocity *u*. Apart from the standard 2 mg/mL 130 cm/h runs there were 2 additional runs per resin, a 2 mg/mL run with 1000 cm/h and a 0.2 mg/mL run with 1000 cm/h.

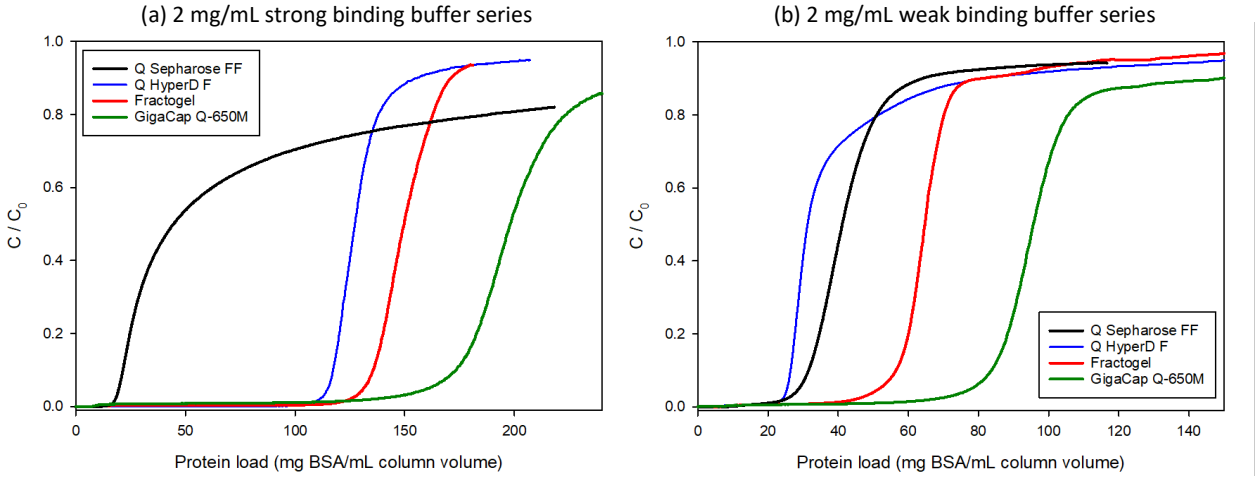

Figure 12: Strong and weak binding buffer breakthrough curve results on the new 0.2 mL columns. Runs were carried out on an ÄKTA Explorer 100 with a linear velocity of 130 cm/h and strong (a) and weak (b) binding buffer conditions. BSA feed concentration was set to 2 mg/mL.

Figure 12 shows the results of the breakthrough experiments on the 0.2 mL columns. The columns had a superior packing quality compared to the 0.5 mL column runs from Figure 9 and Figure 10. This resulted in much smoother curves, with no early breakthroughs. Also, the baseline instability issues mentioned in the conclusion of Section 4.3.2 were removed. When comparing the results of the 0.5 mL column (Figure 12) and the 0.2 mL column (Figure 9 and Figure 10) chromatographic breakthrough curve runs, the basic shape and geometry of the breakthrough curves were comparable. In addition, it was observed that all weak binding buffer offered a significant decrease in protein binding capacity in comparison to their strong binding buffer counterparts. This effect was already hinted in the results of the Isotherm experiments from Section 4.2 as well as from the 0.5 mL column results from Section 4.3.2. Due to the volatile column performance of the 0.5 mL columns, a detailed evaluation was neglected in the previous chapter until more stable results were generated. A quick interpretation of the above graph revealed an increased mass transfer for Q Sepharose Fast Flow when switching from strong binding buffer in Figure 12a to the weak binding buffer in Figure 12b. All other resins offered no improvement in that regard.

Figure 13 and Figure 14 give a detailed picture over the individual resins and the protein behavior when applying the different linear velocities of 130 cm/h and 1000 cm/h in combination with a protein concentration of 2 mg/mL and 0.2 mg/mL. Figure 13 shows the strong buffer results while Figure 14 emphasizes experimental data generated with weak binding buffer.

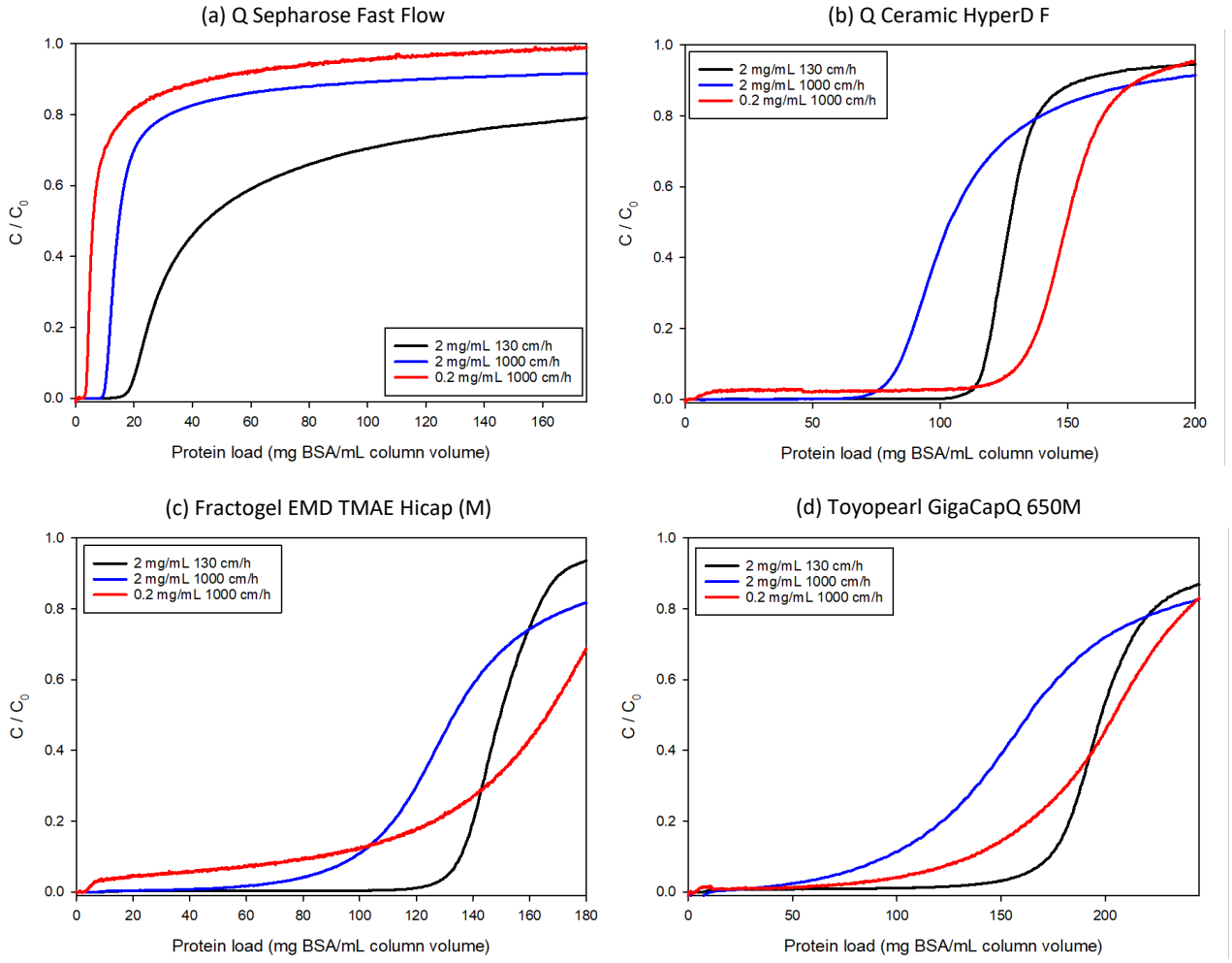

Figure 13: Results of 0.2 mL columns breakthrough curve experiments with strong buffer condition on an ÄKTA Explorer 100. A BSA concentration of 2 mg/mL and 0.2 mg/mL was used for the runs, while varying the linear velocity *u* to 130 cm/h and 1000 cm/h. The varied linear velocity results in a residence time of 27.7 s (130 cm/h) and 3.6 s (1000 cm/h).

Figure 13a features Q Sepharose Fast Flow resin, the results are talked about in detail in Section 4.6.3.3 and corresponding Figure 19. The overall mass transfer in Figure 13a is limited due to the availability of the pores on the resin with the used buffer system.

Figure 13b shows results on Q Ceramic HyperD F resin, reference was taken toward data published from Fernandez, Laughinghouse and Carta[38] in Figure 8a of their publication. They used 50 mM TRIS-HCl at pH 8.5 – 8.6 as buffer system of choice versus the 22 mM TRIS-HCl pH 8.1 used in this dataset, therefore the data was highly comparable. Also, the linear velocity was comparable for the relevant data. The 2 mg/mL 130 cm/h curve seemed comparable to the published dataset (400 cm/h linear velocity in the publication), whereas the 2 mg/mL 1000 cm/h curve did not seem as steep as in the corresponding comparison (7.200 cm/h linear velocity in the publication). Their findings on Q Ceramic HyperD F in the equivalent buffer system reported surface diffusion being the main mode of intraparticle mass transfer. This seemed to match with the data recorded in Figure 13b.

Figure 13c and d seemed to be very similar to each other. This was due to their nature of sharing a very similar chemical structure of grafted polymers. A minor difference was spotted only in detail with the early breakthrough in the 0.2 mg/mL 1000 cm/h curve of the Fractogel dataset or the delayed curve increase in the 2 mg/mL 1000 cm/h Fractogel data versus the Toyopearl data. In these two cases the trend seemed to be that the breakthrough and the overall slope were significantly reduced when increasing the linear velocity incrementally. This especially applied to the 0.2 mg/mL 1000 cm/h curves, which did feature a reduced protein concentration. The changed concentration gradient seemed to affect the reduced diffusional permeation of the protein into the particle directly proportional.

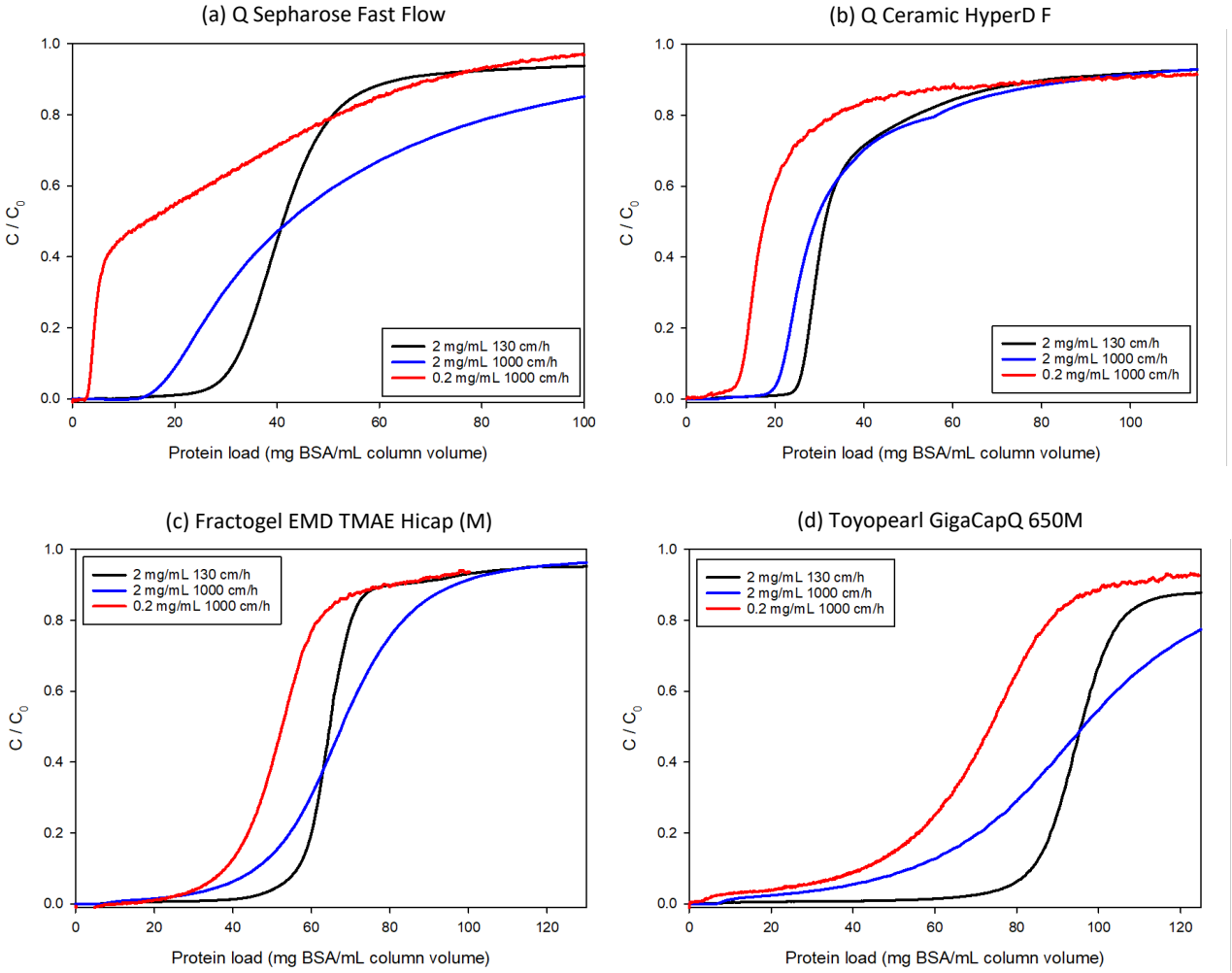

Figure 14: Results of 0.2 mL columns breakthrough curve experiments with weak buffer condition on an ÄKTA Explorer 100. A BSA concentration of 2 mg/mL and 0.2 mg/mL was used for the runs, while varying the linear velocity *u* to 130 cm/h and 1000 cm/h. The varied linear velocity results in a residence time of 27.7 s (130 cm/h) and 3.6 s (1000 cm/h).

The overall pore restrictions, that were hindering the transport under strong binding buffer conditions in Figure 13a didn't apply for the weak binding buffer dataset. The buffer system showed an improved availability of the pores, leading to an increased mass transfer rate. However, this came with an overall reduced protein binding capacity. This effect hinted a mechanistic change when replacing the buffer systems. The shape of the 0.2 mg/mL 1000 cm/h curve was replicated in experimental trials, a reasonable statement for this behavior was not made.

Figure 14b curves all had a similar shape and slope. They slightly differed in curve steepness and a decreased protein binding capacity. Varying the above given parameters only influenced the shape to a minimal degree, therefore the most impact was seen on the protein binding capacity of the column.

As in Figure 13c and d, Figure 14 c and d seemed to share the overall trend of being comparable. However, the curves seemed to be more constricted and steeper in the Fractogel dataset than the corresponding Toyopearl experimental data. The Toyopearl 130 cm/h data seemed also quite comparable to its strong binding buffer counterpart of Figure 13. The order of 0.2 mg/mL 1000 cm/h and 2 mg/mL 1000 cm/h curve appeared to have changed. Therefore, the previous statement that increasing the velocity while keeping the same protein concentration lead to a reduced and slower adsorption rate of protein into the resin particle was made. This admission was also true for Figure 13, but not as intense as in the weak binding buffer case.

It was concluded that the mass transfer of 0.2 mg/mL 1000 cm/h runs in Figure 14 seemed improved in comparison to the 2 mg/mL 1000 cm/h runs from the same Figure. The strong binding buffer 1000 cm/h 0.2 mg/mL runs in Figure 13 showed an increased protein uptake in comparison to their 130 cm/h 2 mg/mL counterpart runs from the same Figure. This phenomenon was however not valid for the Q Sepharose Fast Flow data and was not replicated in the corresponding weak binding buffer results from Figure 14. Therefore, it looked like an exclusive finding to the strong binding buffer system, a reasonable explanation for this behavior was not made.

The chapters conclusion was that the two core problems mentioned in Section 4.3.2 were successfully addressed. By changing the columns, the chromatographic performance was increased significantly while in addition, introducing a linear velocity of 1000 cm/h. The run length was decreased without any negative effect on the chromatographical outcome. One final remark was made towards the introduction of the increased linear velocity of 1000 cm/h as all columns were able to withstand the condition without any problem or loss in separation performance.

4.6 Chromatographic modelling

4.6.1 Pore diffusion model

The Experimental data gathered in Section 4.5 was evaluated using the workflow elaborated in Section 3.2.2.3. Table 4 reveals the numerical fit data parameters when applying the constant pattern solution of the pore diffusion model to the experimental data. The model included external film resistance.

Table 4: Numerical results of strong and weak binding buffer series fitted with the constant pattern solution of the pore diffusion model developed by Weber[26]. The 130 cm/h 2 mg/mL breakthrough curve 0.2 mL column results from Section 4.5 served as foundation for the comparison to the calculated model data. In addition, an analogy between the modelled pore diffusion coefficient and the calculated free solution diffusivity was drawn. The unhindered free solution diffusivity D_0 of BSA is $6.77*10^{-7}$ cm^2/s and was calculated in Section 4.6.3.1.

Buffer system	Resin / protein concentration	D_e (cm^2/s)	Pore diffusion as multitude of free diffusivity D_0	q_m (mg/ cm^3 particle)
Strong binding buffer conditions	Fractogel EMD TMAE Hicap (M)	$2*10^{-6}$	2.95	230
	Q Ceramic HyperD F	$7*10^{-7}$	1.03	193
	Q Sepharose Fast Flow	$3*10^{-8}$ [a]	0.06	---[b]
	GigaCap Q-650M	$2*10^{-6}$	2.95	298
Weak binding buffer conditions	Fractogel EMD TMAE Hicap (M)	$3*10^{-6}$	4.43	99
	Q Ceramic HyperD F	$2*10^{-7}$	0.30	47
	Q Sepharose Fast Flow	$7*10^{-7}$	1.03	63
	GigaCap Q-650M	$8*10^{-7}$	1.18	146

[a] from batch adsorption experiment results as no practicable breakthrough curve pore diffusion model fit was viable

[b] no practicable pore diffusion model fit was viable

When comparing the protein binding capacity q_m from Table 4 with the one from the calculated adsorption isotherm data from Table 2 in Section 4.2, an agreement in data consistency in most cases was seen. The biggest difference in terms of capacity seemed the Q Ceramic HyperD F weak binding buffer (100 mg / cm^3 particle in the adsorption isotherm dataset compared to 47 mg / cm^3 particle in the 0.2 mL column breakthrough run dataset). For the Toyopearl GigaCap Q-650M no experimental isothermal data was available to compare to, fortunately the supplier provided a dataset with capacity values[43]. A static protein binding capacity of 162 mg BSA / mL resin was reported under similar conditions to the strong binding buffer. TOSOH did experiments by using BSA that utilizes a buffer consisting of 50 mM TRIS-HCl, no added NaCl and pH 8.5 while the strong buffer used in this thesis consist of 22 mM TRIS-HCl, no added NaCl and with a pH of 8.1. Assuming a void fraction of 0.35, this resulted in a static binding capacity of 249 mg BSA / cm^3 particle volume. This differed by a margin of 16% from the dynamic binding capacity of 298 mg / cm^3 particle determined in Table 4. For the weak

binding buffer (50 mM HEPES, 65 mM NaCl and pH 7.0) no literature or reference was retrieved to directly compare the results to.

To show how these pore diffusion values of Table 4 behaved in comparison to the unhindered free solution diffusivity D_0 of BSA ($6.77*10^{-7}$ cm^2/s; calculated in Section 4.6.3.1) a comparison was drawn. Usually, the pore diffusion is slower as more hindered by several restraining effects that can be found in the resin in comparison to the unhindered free diffusivity taking place in solution. Especially Q Sepharose Fast Flow showed a reduced pore diffusion in comparison to the free diffusivity. This result was supported by the findings in Figure 12a, where the resin showed a very hindered breakthrough curve indicating a slow mass transfer. These findings revealed that the mass transfer was not rendered only via pore diffusion, but by another mechanisms as surface diffusion that was the main driving force.

The contrary example was found on the GigaCap Q-650M as well as the Fractogel EMD TMAE Hicap (M) weak binding buffer results. They showed a significant increase in protein mass transfer, resulting in an amplification of up to ~3 and ~4.5 times. These results were not explainable by pore diffusion only, usually the pore limited such diffusional activity. Therefore, these findings indicated that the protein adsorption on the resin was carried out via pores and in additional with diffusion via the surface. This did result in a parallel diffusion model for these scenarios.

4.6.2 Surface diffusion model

Previous fit attempts to harmonize experimental data with the pore diffusion model were done using the assumption that the concentration gradient based main linear driving force was set up in the pores. The surface diffusion model describes the reversible attachment onto the surface of the solid phase based on the concentration gradient of the bound protein as the single dominant force of diffusion. The model includes external film resistance. Experimental data was evaluated using the workflow elaborated in Section 3.2.2.4.

Table 5: Numerical results of strong and weak binding buffer series fitted with the analytical solution developed by Yoshida[28] of the surface diffusion model. The 130 cm/h 2 mg/mL breakthrough curve 0.2 mL column results from Section 4.5 served as foundation for the comparison to the calculated model data.

Buffer system	**Resin / protein concentration**	**D_s (cm²/s)**	**q_m (mg/cm³ particle)**
Strong binding buffer conditions	Fractogel EMD TMAE Hicap (M)	$5*10^{-9}$	224
	Q Ceramic HyperD F	$3*10^{-9}$	197
	Q Sepharose Fast Flow	$1.3*10^{-9}$ [a]	---[b]
	GigaCap Q-650M	$3*10^{-9}$	300
Weak binding buffer conditions	Fractogel EMD TMAE Hicap (M)	$7*10^{-9}$	100
	Q Ceramic HyperD F	$3*10^{-9}$	54
	Q Sepharose Fast Flow	$9*10^{-9}$	65
	GigaCap Q-650M	$6*10^{-9}$	145

[a] from batch adsorption experiment results as no practicable breakthrough curve solid diffusion model fit was viable

[b] no practicable solid diffusion model fit was viable

As can be observed from Table 5, the assumption postulated in Section 2.3.2.2.2 that the surface diffusion coefficient D_s differed from the pore diffusion coefficient D_e by a magnitude of up to ~10^2 proved to be correct. This resulted in a much slower uptake of the protein by the particle surface than over the available pores. All calculated surface diffusion coefficients were in the area between $3*10^{-9}$ cm²/s and $9*10^{-9}$ cm²/s. There also seemed no trend that was identified between strong and weak buffer experiments with the surface diffusion coefficient D_s. In terms of protein capacity q_m, no difference was spotted when comparing the pore (Table 4) and the surface diffusion model (Table 5).

4.6.3 Parallel diffusion model

Certain experimental data gathered in Section 4.5 were compared to the data produced by the CADET Web toolkit to generate a parallel diffusion model comparison and make model predictions as well as basic mechanistic revealing. To further simplify the modelling process, a 1-component 1-loading step breakthrough curve based on the Langmuir general rate model was designed and used. The workflow of the simulation is described in Section 3.2.2.5 of this thesis in more detail.

The axial dispersion was calculated according to the workflow described in Section 3.2.2.2. Fitting of the Q Sepharose weak binding buffer 130 cm/h data in TableCurve 2D resulted in the best regression (r^2=0.9993) fit. The parameters from the EMG model were determined as *a* (1.693), *b* (200.648), *c* (3.776), *d* (0.574) and *e* (0.757). The calculation of the first momentum μ (retention time) and second momentum σ (variance) was according to the following equations:

$$\mu = c + e \tag{4.1}$$

$$\sigma = d^2 + e^2 \tag{4.2}$$

This resulted in a HETP of $4*10^{-2}$ according to Equation 2.7, which further translated into an axial dispersion of $7.2*10^{-8}$ m²/s with the help of Equation 2.8. This parameter was used for all CADET simulations from Section 4.6. The particle porosity was assumed as 0.72 for the Q Sepharose Fast Flow and 0.71 for the Fractogel EMD TMAE Hicap (M) resin according to CADET simulation experiments, a column void fraction *ε* of 0.30 was assumed for the simulations. All other necessary parameters for the simulations were used as described in the following chapters of this work.

As in Section 4.3.1, the film mass transfer *kf* was calculated according to Equation 2.12. The appropriate resin particle diameter d_p was according to 3.1.1.1, the kinematic viscosity *v* was 0.01 cm²/s, a free diffusivity D_0 was calculated as $6.77*10^{-7}$ cm²/s (from Section 4.6.3.1). Table 6 gives an overview over the different film mass transfer k_f in dependency on the linear velocity *u*.

Table 6: Calculated film mass transfer *kf* values for all used resins using different linear velocities *u*. The film mass transfer is a required parameter input for all upcoming simulations of this section to generate proper parallel diffusion curves.

	k_f (cm/h)			
Linear velocity *u* (cm/h)	**Q Sepharose Fast Flow**	**Fractogel EMD TMAE Hicap (M)**	**Q Ceramic HyperD F**	**GiGaCap Q-650M**
6	$1.4*10^{-4}$	---	---	---
20	$2.5*10^{-4}$	---	---	---
130	$6.5*10^{-4}$	$7.2*10^{-4}$	$8.7*10^{-4}$	$7.1*10^{-4}$
500	$1.3*10^{-3}$	$1.4*10^{-3}$	$1.7*10^{-3}$	$1.4*10^{-3}$
1000	$1.8*10^{-3}$	$2.0*10^{-3}$	$2.4*10^{-3}$	$2.0*10^{-3}$

4.6.3.1 Calculation of essential BSA constants and coefficients

Recalling the simplified form of the Tyn Gusek relation (Equation 2.22) and using the adequate parameters for the experiments with BSA (η = 1 mPa*s, T = 298 K, M_r = 66470 Da) resulted in a calculated free solution diffusivity D_0 of 6.77*10^{-7} cm^2/s for BSA.

This calculated free solution diffusivity parameter was used in combination with the Boltzmann constant in the Stokes-Einstein equation (Equation 2.21). This resulted in a hydrodynamic radius r_h of 3.23 nm for a single BSA molecule.

The ratio of hydrodynamic protein radius to resin pore radius λ_m was used for the calculation of the diffusional hindrance coefficient ψ_P. For that, the radius of the pore matrices was needed. According to Carta and Jungbauer[4], which reported a Q Sepharose Fast Flow pore radius of 30 nm (Table 3.13 in the cited publication) lead to a λ_m ratio of 0.11. The diffusional hindrance coefficient ψ_P depends on λ_m, in case of λ_m < 0.2 Equation 2.18 was recommended. By solving that calculation, a diffusional hindrance coefficient ψ_P of 0.56 was evaluated.

To calculate the effective pore diffusivity D_e, Equation 2.17 was used. ε_p was assumed as 0.84 from Zhang et al.[3] while a tortuosity factor τ_p of 1.5 was assumed. An effective pore diffusivity of 2.2*10^{-7} cm^2/s was calculated using this method.

4.6.3.2 Prediction and evaluation of Q Sepharose Fast Flow weak binding buffer

The upcoming parallel diffusion modelling concept in this Section consisted of the verification of the apparent effective diffusion coefficient $\widehat{D_e}$ by utilizing the parallel diffusion workflow described in Section 3.2.2.5. The CADET Web Interface only allowed the input of the pore and surface diffusion parameters; it was not possible to enter a value for the apparent effective diffusion coefficient $\widehat{D_e}$ on its own. To bypass this problem the unknown surface diffusion D_s parameter was expressed via Equation 2.34 and entered with the other known parameters. The calculation served as a proof of concept for the question if this was overall possible and to examine up to which extent the calculated result corresponded with the simulations.

For calculating the extent of surface diffusion in the apparent effective diffusion coefficient $\widehat{D_e}$ Equation 2.34 was used. To estimate a value for the parallel diffusion parameter, the determined value of the weak binding buffer Q Sepharose Fast Flow 130 cm/h parameter from Table 4 was used in the equation as the apparent effective pore diffusion $\widehat{D_e}$ (7.0*10^{-7} cm^2/s). Using a protein feed concentration of 2 mg/mL, this resulted in a surface diffusion coefficient of 1.53*10^{-8} cm^2/s. This value seemed reasonable since the resins previous surface diffusion coefficients D_s from Table 5 appeared as 9*10^{-9} cm²/s. The protein binding capacity q_m was assumed as 63 mg/cm³ particle, this value was based on the weak binding buffer Q Sepharose Fast Flow 130 cm/h fit results from the experiments in Table 4. This was confirmed with the data from the isothermal experiments in Table 2 (66 mg/cm³ particle) as well as the one from the batch adsorption experiments from Table 3 (65 mg/cm³ particle).

The calculated results and the resulting parallel diffusion curve are shown in Figure 15. The fit of the pore diffusion model was added as comparison. The calculated parallel diffusion model curve only differed slightly from the experimental data. After further fitting attempts it was concluded that adjusting the surface diffusion coefficient D_s only modified the beginning and the ending of the uptake curve. Finetuning the surface diffusion coefficient D_s did not seem to change the symmetry of the breakthrough curve in a major way.

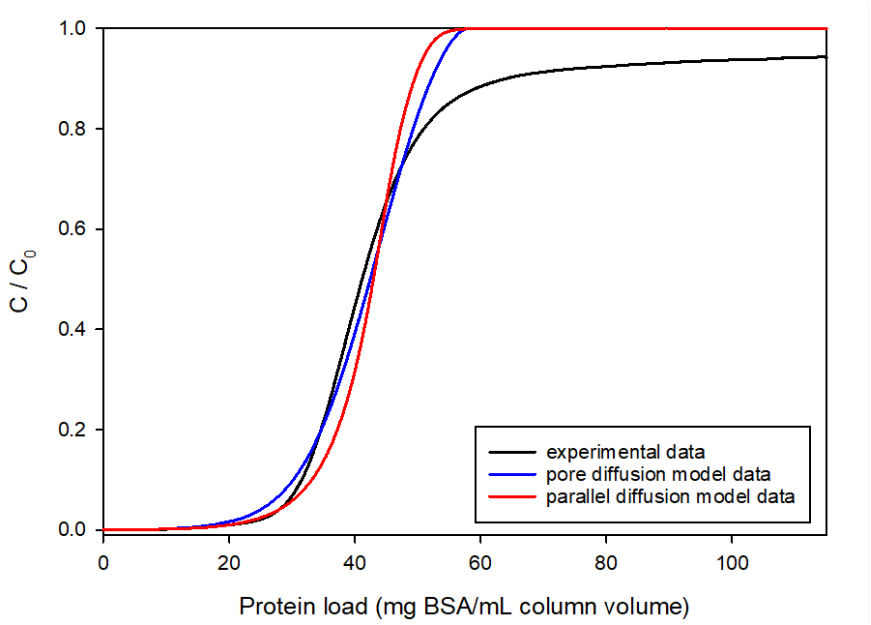

Figure 15: Comparison of Q Sepharose Fast Flow weak binding buffer experimental data from Figure 12b to the pore diffusion model data from Table 4 and the calculated parallel diffusion model. Protein capacity of the parallel diffusion model data needed adjustment up to 150 mg/ml to match with experimental data. Feed concentration was 2 mg/mL, linear velocity was set to 130 cm/h, any experimental data was recorded on the corresponding 0.2 mL column using a ÄKTA Explorer 100.

The experimental data upper curve reached its C/C_p equilibrium summit at ~ 0.9, therefore never able to extend upon the calculated fit data. This did affect the match with the calculated model that always extended to a full saturation of C/C_p. However, if the maximum of the experimental data got an artificial enhanced up to a $C/C_p = 1$, there would be a better comparison. Figure 16 displays such an artificial enhance in comparison with the calculated pore diffusion model data. As one can see there was a slight improvement, comparability of the upper curve was increased. However, the model curve seemed to steepen overall, indicating a slightly too fast calculated uptake rate.

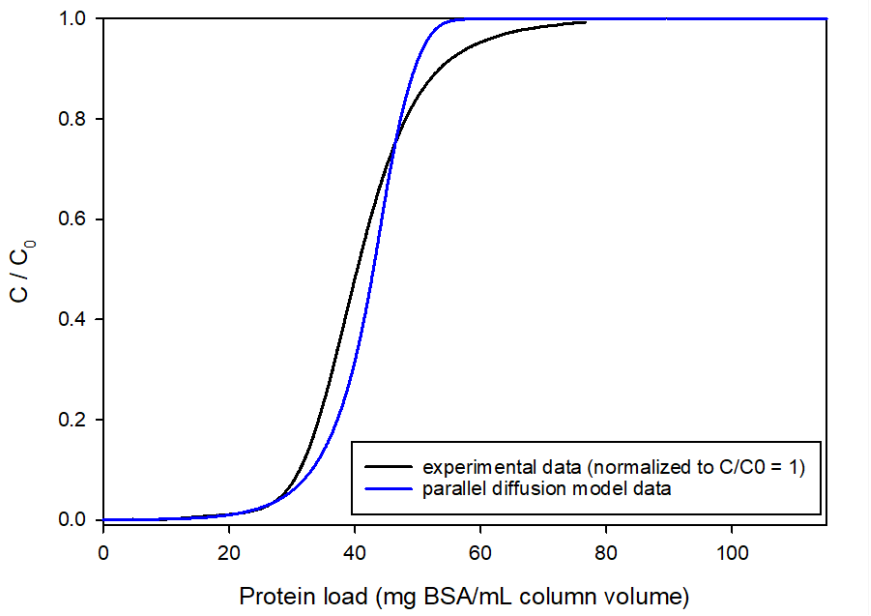

Figure 16: Comparison of calculated parallel diffusion results from Figure 14 to the $C/C_p = 1$ normalized Q Sepharose Fast Flow weak binding buffer experimental data from Figure 12b. The calculated parallel diffusion model curve does not fit the experimental data completely, leaving room for improvement by adjusting the calculated parameters.

An even better fit was reached when optimizing the parameters by hand, they can be found in Table 7. The algorithm based iterative fitting of the offline core CADET toolkit was not available in the web version, therefore fitting by hand was needed. The resulting curve of this fit can be seen in Figure 17.

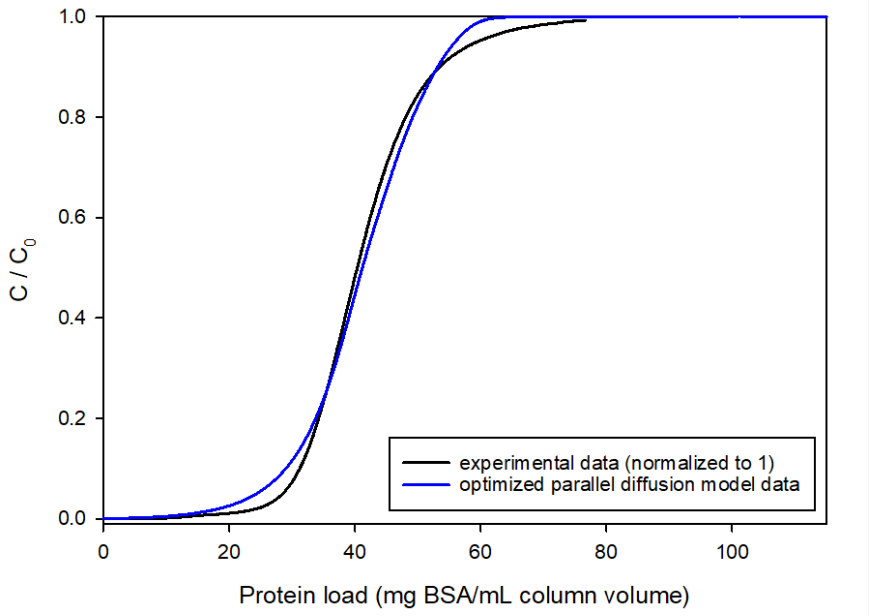

Figure 17: Comparison of optimized pore diffusion model results to the $C/C_p = 1$ normalized Q Sepharose Fast Flow weak binding buffer experimental data from Figure 12b. The optimized parameters guarantee a better match than the one in Figure 16.

Table 7: Q Sepharose Fast Flow weak binding buffer parallel diffusion fitting parameter that were determined in this Section. The calculated parameters are in comparison to the optimized parameter to offer a better outline of the data.

	Effective pore diffusivity D_e (cm²/s)	**Solid phase diffusion coefficient D_s (cm²/s)**	**Apparent effective pore diffusion $\widehat{D_e}$ (cm²/s)**	**q_m (mg/ cm³ particle)**
Calculated and assumed parameter	$2.2*10^{-7}$	$1.5*10^{-8}$	$7.0*10^{-7}$	63
Optimized parameter	$1.8*10^{-7}$	$1.0*10^{-9}$	$2.6*10^{-7}$	65

As postulated, the calculated effective pore diffusivity D_e was slightly too fast, resulting in a too steep curve. Fitting by hand allowed the generation of optimized fitting parameter, these were quite close to the calculated ones.

4.6.3.3 Prediction and evaluation of Q Sepharose Fast Flow strong binding buffer

A problem that occurred when trying to apply a fit to the strong binding buffer experimental dataset from Figure 12a was, that none fit could be made as there is no model that allows for a possible fit in the case of reduced solute surface transport with a linear velocity *u* of 130 cm/h and the given conditions. One possible solution for this was to reduce the overall linear velocity *u* of the breakthrough experiment. This resulted in a much slower migration of the protein over the surface, therefore reducing the hindering effects. Figure 18 gives an overview of such an experiment with varied linear velocities of *u*. Figure 18a displays the ineffectiveness of an attempt to harmonize a fit with the previously introduced 130 cm/h linear velocity *u* experimental dataset. Figure 18b shows a rapid decrease in speed of linear velocity *u*, applying 6 cm/h overall and therefore allowing a fit to calculate the parameter. Figure 18c displays the fit result when operating at a slightly higher linear velocity *u* of 20 cm/h. This also allowed for a good fit as the pore diffusion model was applied successfully to both datasets in Figure 18a and Figure 18b. All data from Figure 18 was fitted with the corresponding pore diffusion model that utilizes the constant pattern solution from Section 2.3.2.2.1.

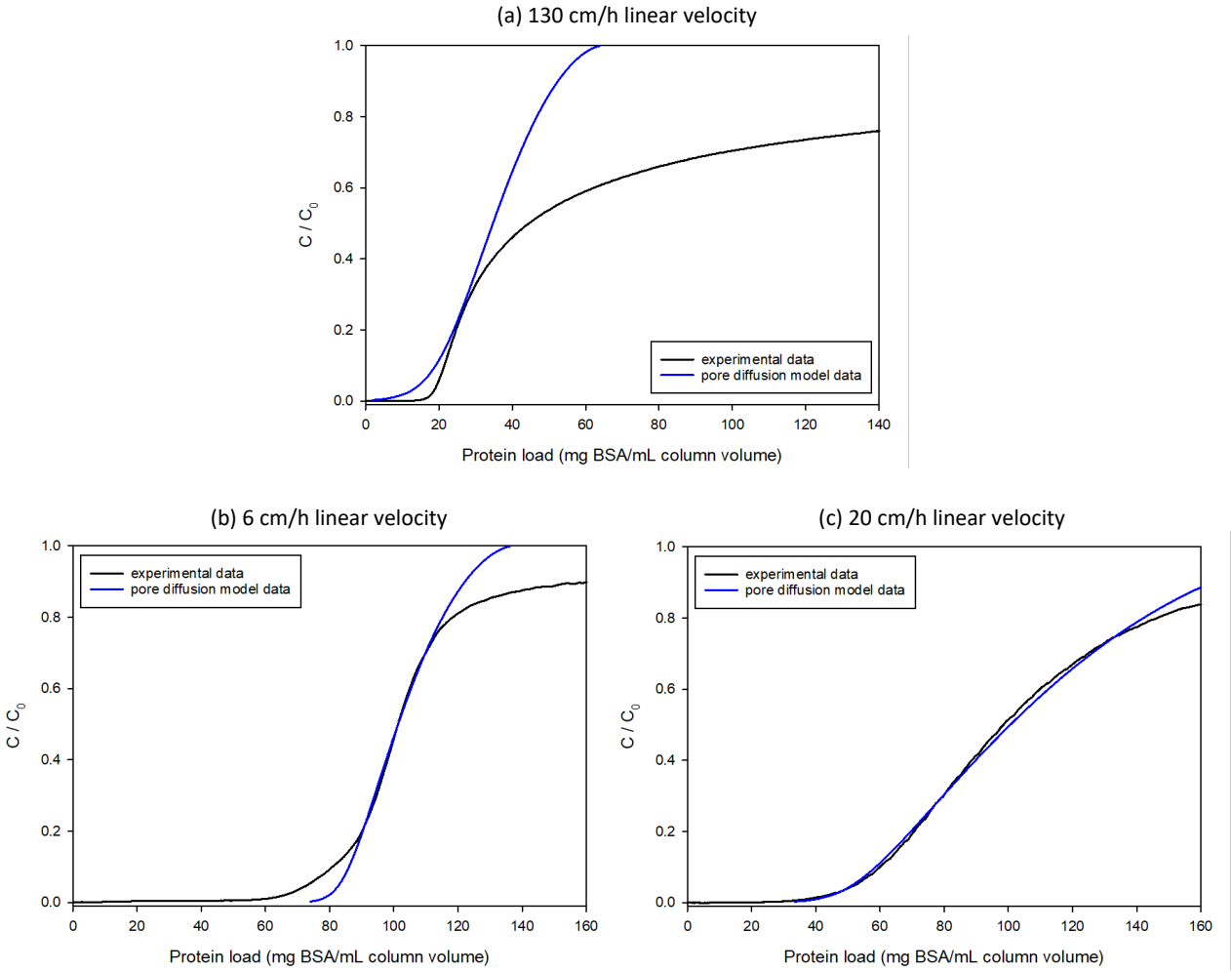

Figure 18: Comparison of different linear velocities of Q Sepharose Fast Flow strong binding buffer breakthrough curve. The aim was to find experimental conditions for a good fit, as previous fit of 130 cm/h data was not possible. Protein feed was set to 2 mg/mL, the experiments were carried out on 0.2 mL columns with an ÄKTA Explorer 100.

The determined fit data can be observed in Table 8. As can be seen from Figure 18a and Figure 18b, the fit data resulted in a slower mass transfer than expected, resulting in a small pore diffusion coefficient D_e but great reproducibility and similar results over the experiments.

Table 8: Protein capacity q_m and pore diffusion coefficient D_e fit parameters results from Figure 18. The experimental velocity was reduced to generate an adequate fit as these input parameters are required in Equation 2.34. The 6 cm/h and 20 cm/h results show a great accordance and will be used for further calculations.

Linear velocity *u* (cm/h)	**Protein binding capacity q_m (mg/cm³ particle)**	**Pore diffusion coefficient D_e (cm²/s)**
6 cm/h	160.0	$2.8*10^{-8}$
20 cm/h	162.0	$3.1*10^{-8}$
130 cm/h	---[a]	---[a]

[a] no practicable pore diffusion model fit was viable

Figure 19 gives an overview of the different strong binding buffer mass transfer mechanisms when applying different paces of the linear velocities *u*. The 6 cm/h as well as 20 cm/h curve represented the experimental data and their corresponding fits from Figure 18. It was assumed to be pore diffusion; this phenomenon has already been addressed in this Section.

The 130 cm/h line represented the experimental data from Section 4.5, which did not allow a suitable fit with the given models. It was assumed to be surface diffusion, the solute transport through the pores was substantially hindered. Both of these annotations were confirmed by Zhang et al.[3] Figure 5b of the publication gave an summary over this phenomena by the usage of CSLM images. These displayed the saturation of the resin particle over a given time course. They were noted by the authors for their very low weak interaction between the pore and its ligands. Most likely this resulted in a saturation of the particle over the surface. However, their setup used a BSA protein concentration of 0.5 mg/mL instead of the 2 mg/mL used in the Figure 19 experimental results. This did impact the influence of the concentration gradient that powered the driving force.

The 1000 cm/h line represented an experiment that was done with the same boundary conditions as the other experiments in Figure 19, except an even further enhanced linear velocities *u*. This resulted in a residence time of ~ 3.6 sec. The solute was transferred so fast over the particles, it further enhanced the effect of reduced solute uptake via surface diffusion that was described with the 130 cm/h curve.

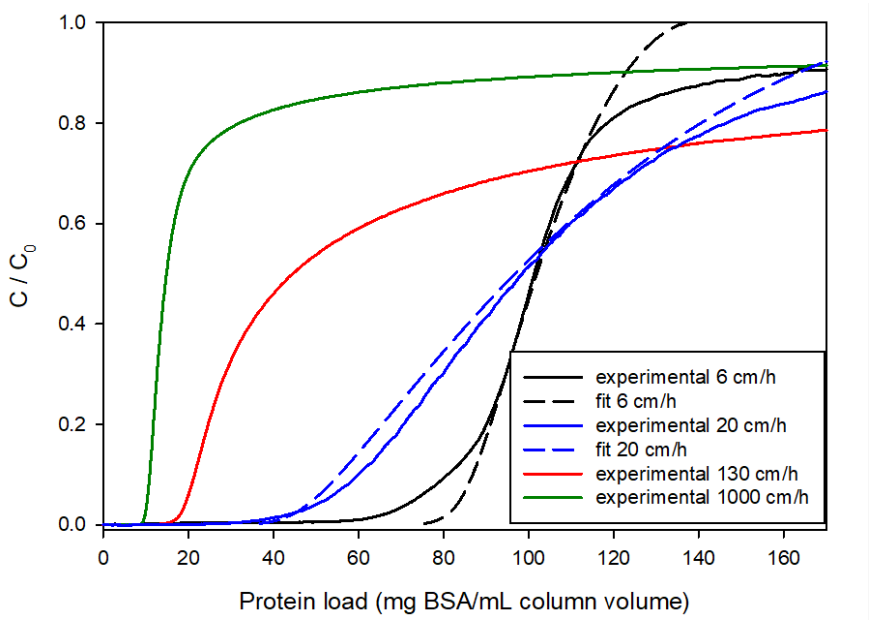

Figure 19: Summary of varying linear velocity *u* Q Sepharose Fast Flow strong binding buffer experiments and the corresponding pore diffusion model fitting attempts of the 6 cm/h and 20 cm/h low velocity experiments. There seems to be a significant shift in mass transfer models on the go as can be seen on the symmetry and behavior of the curves. For the 130 cm/h and 1000 cm/h experimental data no model fit was possible.

The strategy of lowering the overall velocity of the experiments to remove the hindered diffusion was successful. An apparent effective pore diffusion of $2.95*10^{-8}$ cm²/s was estimated this way. It was only possible to generate a fit for the 6 cm/h and 20 cm/h experimental data using the pore diffusion model. A possible upscale of this model however did not bring any promising results and was therefore neglected in this thesis.

4.6.3.4 Prediction and evaluation of Q Ceramic HyperD F

As in Figure 13b elaborated, concluded in Section 4.5 and further supported by the findings of Fernandez and coworkers[38] surface diffusion seemed to be the dominating form of mass transfer for Q Ceramic HyperD F for both binding buffer systems. The corresponding fit data can be found in Table 5 with a surface diffusion coefficient D_s of $3*10^{-9}$ cm²/s for both buffer systems. This also indicated that a change of the buffer system did not improve or worsen the mass transfer rate. Protein binding capacity q_m was estimated with 197 mg/cm³ particle for the strong binding buffer and 54 mg/cm³ particle for the weak binding buffer. This data is valid for a linear velocity u of 130 cm/h.

Figure 20 displays a possible projection if the same fit parameters are used but with a different linear velocity u of 1000 cm/h and/or a varying protein feed concentration c_p of 2 mg/mL or 0.2 mg/mL. This most simple method of an velocity upscale while varying the protein concentrations used Yoshidas surface diffusion model[28] with the workflow elaborated in Section 3.2.2.4. The 130 cm/h experimental curve and the appropriate fit in Figure 20 of the strong and weak binding buffer are for comparison.

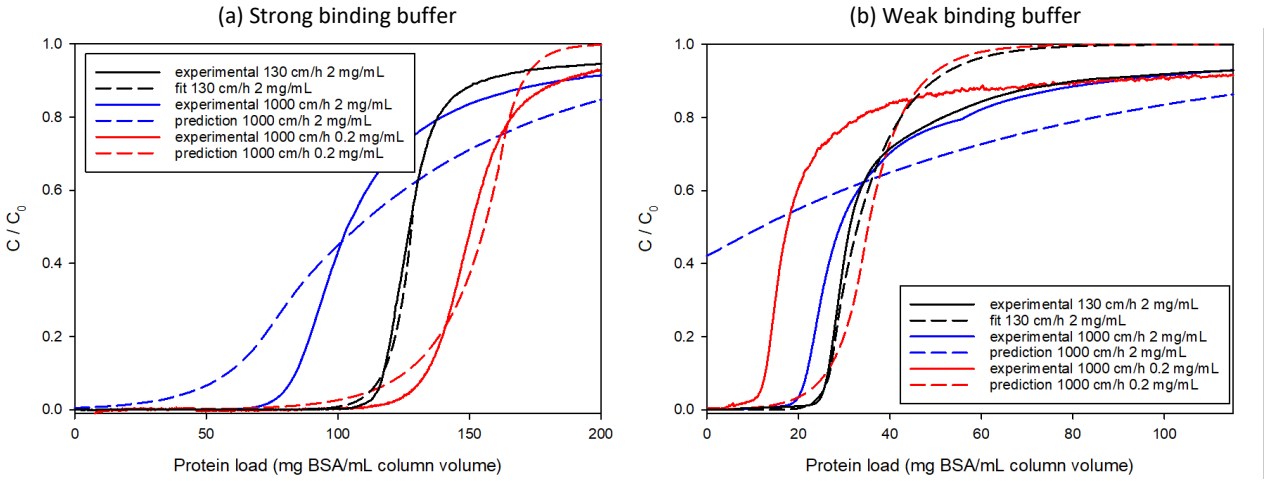

Figure 20: Q HyperD F strong and weak binding buffer 1000 cm/h velocity predictions. These model predictions are based on parameter of experimental data from Figure 12a and Figure 12b that has been fitted using the surface diffusion model as in Table 5. In addition, the protein feed concentration of these predictions was varied to 2 mg/mL and 0.2 mg/mL. The predictions were based on a surface diffusion coefficient of $3*10^{-9}$ cm²/s

Figure 20a shows an overall acceptable prediction, especially at low protein concentrations of 0.2 mg/mL the model seemed superior. The predicted 1000 cm/h with 2 mg/mL (dotted line) seemed to match in protein binding capacity. However, a certain inconsistency was spotted when looking at the compliance of the curves. A higher diffusion coefficient was needed to fix this mismatch, which would result in an increased steepness and gain of the breakthrough curve. Figure 20b gives an example where the mathematical model reached its limits, specifically with the predicted 1000 cm/h 2 mg/mL (dotted line). More parameters finetuning and experiments to gather more insight into this phenomenon were needed to propose a solution to this problem. The 0.2 mg/mL prediction didn't seem to deviate like its 2 mg/mL counterpart, the protein binding capacity was rearranged by ~ 20 mg/mL. The overall curve trend seemed comparable.

To summarize the Q Ceramic HyperD F experimental results, the rate of diffusion did not change with a variation of linear velocity or a change of the buffer system, it stayed constant. The uptake speed via the particle surface was therefore limited and did not scale, it did only affect the total protein uptake capacity of the resin. In terms of predictions, the strong binding buffer predictions proved to be reliable to a certain extent about the shape and trend of the curve. It also gave hints about how Q HyperD F seemed to behave at lower protein concentrations.

4.6.3.5 Prediction and evaluation of Fractogel EMD TMAE Hicap (M) strong binding buffer

As the pore diffusion as multitude of free diffusivity D_0 evaluation of Fractogel experimental data in Section 4.6.1 already proved, a parallel diffusional mass transfer was assumed. For the strategy of calculating the effective diffusion coefficient $\widehat{D_e}$ no reliable literature data was found for the essential parameters needed in the calculation. Therefore, the primary aim was to determine the ratio of pore to surface diffusion in the parallel diffusion model applied to the Fractogel resin data. Later, the parameters were used for a velocity upscale. To accomplish this goal the experimental data from Section 4.5 was fitted in the CADET web interface by iterative fitting. The algorithm based iterative fitting of the offline core CADET toolkit was not available in the web version. The results of this method can be observed in Figure 21. The corresponding fitting data for the parallel diffusion model as well as the other two models for comparison can be found in Table 9. All film mass transfer coefficients used in this Section have been previously calculated in Table 6.

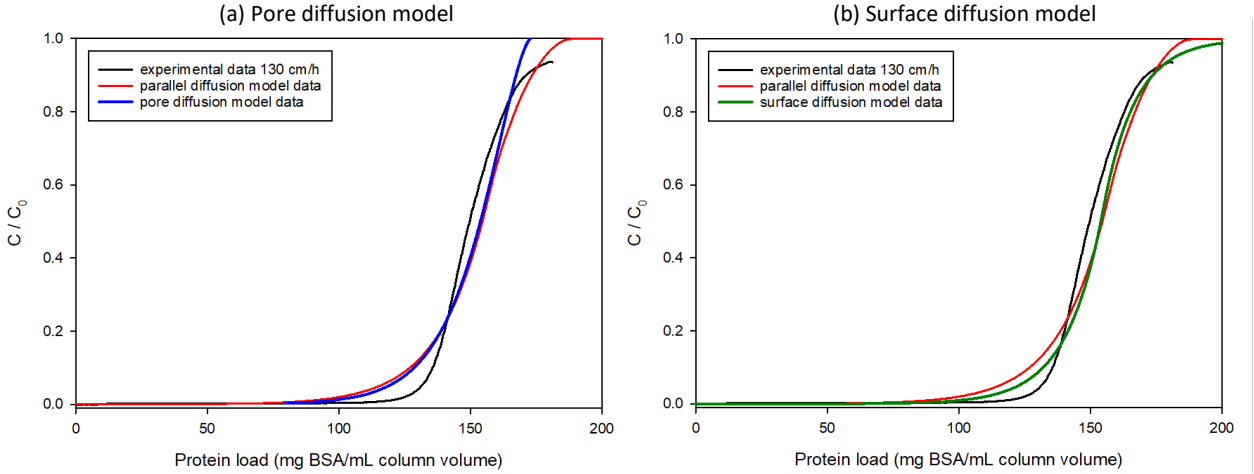

Figure 21: Iterative determined parallel diffusion model parameters in comparison with the pore and surface diffusion model versus the experimental data from Section 4.5 in strong buffer environment. All data was done with a linear velocity of 130 cm/h and a protein feed concentration of 2 mg/mL.

Table 9: Fractogel strong binding buffer fitting parameters for 130 cm/h experimental data from Section 4.5. The parallel diffusion fit parameters were generated through an iterative approach where the experimental data was fitted with the model until an acceptable fit was rendered. The pore and surface diffusion model parameters from Section 4.6.1 as well as from Section 4.6.2 are depicted for the purpose of comparison.

Fitting method	D_e **(cm²/s)**	D_s **(cm²/s)**	q_m **(mg/ cm³particle)**
Parallel diffusion model	$2*10^{-7}$	$2*10^{-9}$	228.5
Pore diffusion model	$2*10^{-6}$	---	230
Surface diffusion model	---	$5*10^{-9}$	227

As can be seen from Table 9 and already explained in the evaluation of Section 4.6.1, the pore diffusion model offered a very high rate of diffusion. These high rates would only be valid in theory, practical they are quite unlikely to achieve under the given conditions. It was therefore believed that a parallel diffusion contribution was involved, this proposition was supported by the parameters calculated with the help of the parallel diffusion model. Figure 21a offers a rendering of the pore diffusion model and the parallel diffusion model compared to the experimental data. Figure 21b displays that same experimental data and parallel diffusion model against the surface diffusion model. As can be observed in Figure 21 there seems to be no ideal fit for this case of experimental data, even the parallel diffusion fit allowed no ideal solution by finetuning of the D_e and D_s parameters.

Figure 22 hints the inaccuracy of the model if just the linear velocity u and the previously calculated film mass transfer coefficient k_f were upscaled to 1000 cm/h and $2*10^{-3}$ cm/s. The approach of upscaling the velocity and film mass transfer of the parallel diffusion curve did not work. The pore diffusion coefficient D_e and surface diffusion coefficient D_s in the parallel diffusion model had to be fitted by hand. This was different to the results of Q HyperD F in Section 4.6.3.4, where the diffusion constant was unrelated to the velocity and did not scale with it. The corresponding pore (Figure 22a) and surface diffusion (Figure 22b) fits were also adjusted to the new linear velocity u.

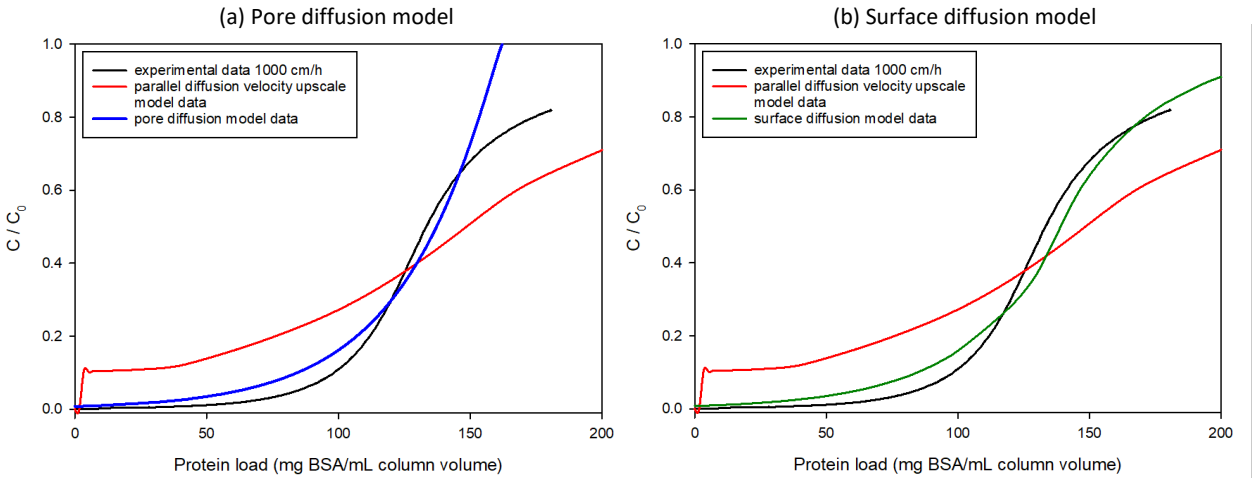

Figure 22: Velocity and film mass transfer coefficient upscaled parallel diffusion model parameters in comparison with the pore and surface diffusion model versus the experimental data from Section 4.5 in strong buffer environment. All data was done with a linear velocity of 1000 cm/h and a protein feed concentration of 2 mg/mL.

With these changes and after finetuning steps it was possible to generate the fitting displayed in Figure 23. The corresponding fitting data for these models can be found in Table 10. The high diffusion rate evaluated with the pore diffusion model was caused by the high velocity of 1000 cm/h applied in the experiment. The assumption that the film mass transfer coefficient k_f can be determined by simple calculation proved to be correct.

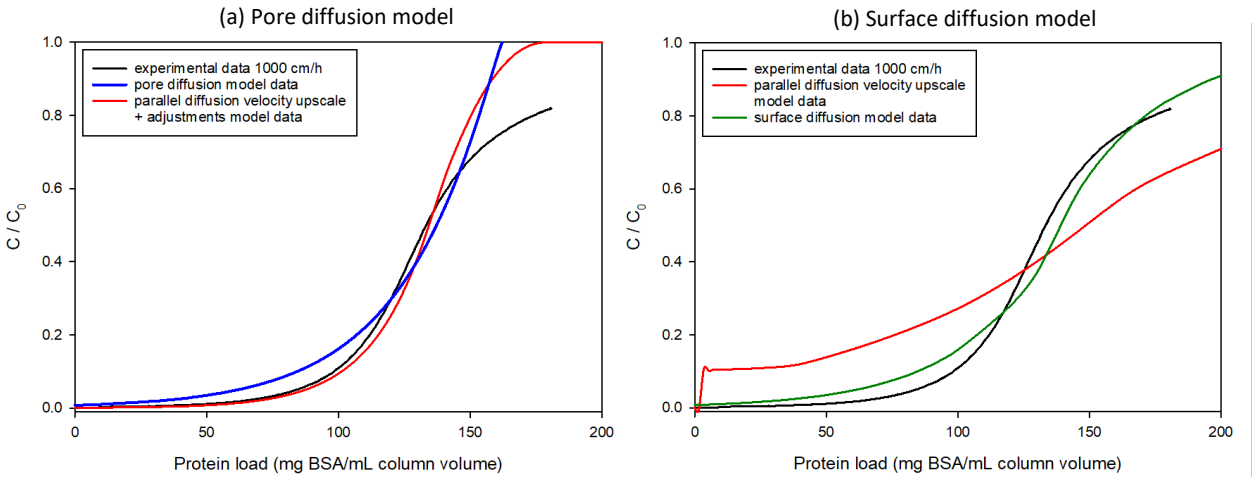

Figure 23: Iterative determined parallel diffusion model parameters in comparison with the pore and surface diffusion model versus the experimental data from Section 4.5 in strong buffer environment. All data was done with a linear velocity of 1000 cm/h and a protein feed concentration of 2 mg/mL.

Table 10: Fractogel strong binding buffer fitting parameters for 1000 cm/h experimental data from Section 4.5. The parallel diffusion fit parameters were generated through an iterative approach where the experimental data was fitted with the model until an acceptable fit was rendered. The pore and surface diffusion model parameters are from Section 4.6.1 as well as from Section 4.6.2 and depicted for purpose of comparison.

fitting method	D_e (cm²/s)	D_s (cm²/s)	q_m (mg/ cm³particle)
Parallel diffusion model	$1*10^{-6}$	$9*10^{-9}$	197.5
Pore diffusion model	$5*10^{-5}$	---	195
Surface diffusion model	---	$1*10^{-8}$	200

To conclude, it was possible to find a good fit for the Fractogel strong binding buffer parallel diffusion experimental data. Due to the complexity of the calculation as well as the several hurdles on the experimental data making predictions for this case proved to be difficult for this case, these did not work out as intended.

4.6.3.6 Prediction and evaluation of Fractogel EMD TMAE Hicap (M) weak binding buffer

This section serves to understand if the same behavior and assumptions from the strong binding buffer findings in Section 4.6.3.5 were appropriate for the weak buffer conditions or if there were any deviations from the findings in Section 4.6.3.5. All film mass transfer coefficients used in this Section have been previously calculated in Table 6. Figure 24 gives a representation of the parameters (u = 130 cm/h, k_f = 7,2*10^{-4} cm/s, c_p = 2 mg/mL) as have been used in strong binding buffer from Section 4.6.3.5 but with weak binding buffer conditions applied to the corresponding mass transfer models.

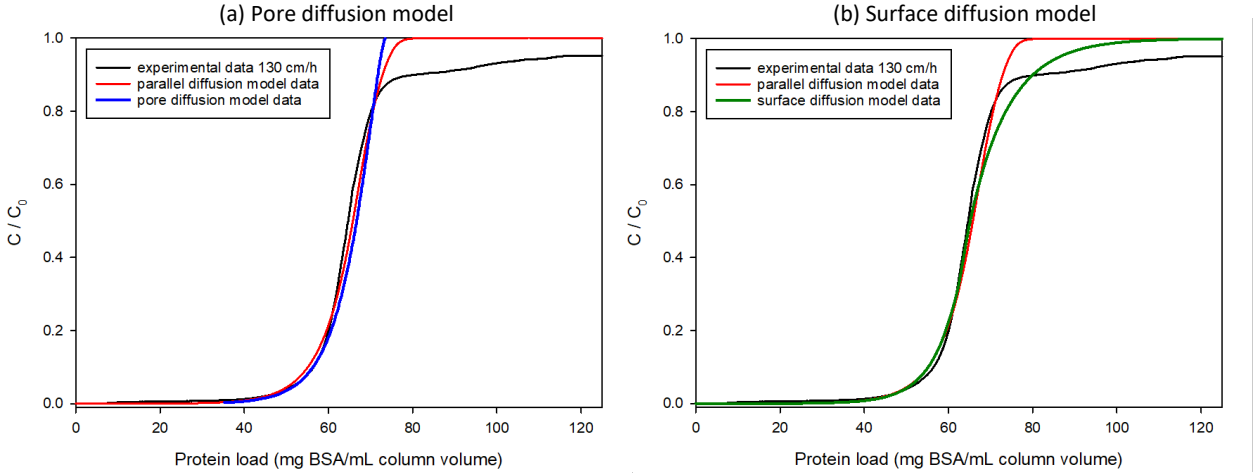

Figure 24: Iterative determined parallel diffusion model parameters in comparison with the pore and surface diffusion model versus the experimental data from Section 4.5 in weak buffer environment. All data was done with a linear velocity of 130 cm/h and a protein feed concentration of 2 mg/mL.

Table 11: Fractogel weak binding buffer fitting parameters for 130 cm/h experimental data from Section 4.5. The parallel diffusion fit parameters were generated through an iterative approach where the experimental data was fitted with the model until an acceptable fit was rendered. The pore and surface diffusion model parameters from Section 4.6.1 as well as from Section 4.6.2 are depicted for the purpose of comparison.

fitting method	D_e (cm²/s)	D_s (cm²/s)	q_m (mg/ cm³particle)
Parallel diffusion model	$5*10^{-7}$	$7*10^{-9}$	92
Pore diffusion model	$3*10^{-6}$	---	99
Surface diffusion model	---	$7*10^{-9}$	100

As a matter of lacking input parameters these had to be determined by the method of iterative fitting. The results of this procedure and the numerical values of the corresponding other mass transfer models are depicted in Table 11.

A new linear velocity *u* of 1000 cm/h was chosen and reused into the model. All other parallel diffusion parameters were unchanged as to Table 11. The results of this velocity upscale can be observed in Figure 25.

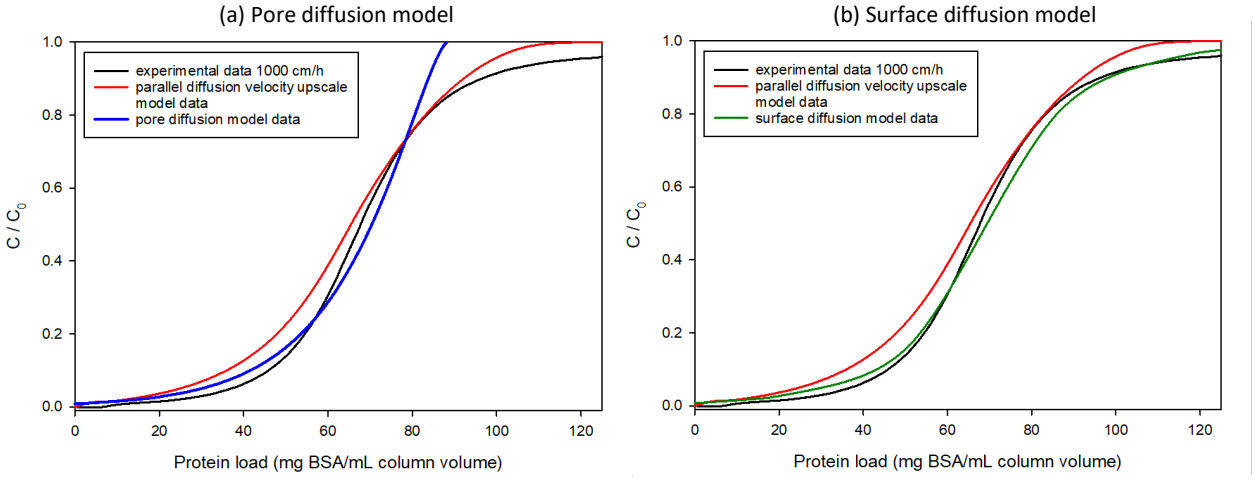

Figure 25: Velocity and film mass transfer coefficient upscaled parallel diffusion model parameters in comparison with the pore and surface diffusion model versus the experimental data from Section 4.5 in weak buffer environment. All data was done with a linear velocity of 1000 cm/h and a protein feed concentration of 2 mg/mL.

A similar result to Figure 22 was found, however the scalability of the weak buffer system seemed more likely than the corresponding strong binding buffer system. Finetuning of the fit by hand revealed the results in Figure 26. The numerical parameters result of all the fits can be monitored in Table 12. The high diffusion rate evaluated with the pore diffusion model was caused by the high velocity of 1000 cm/h applied in the experiment. The values determined by the iterative approach to the parallel diffusion model seemed more realistic and plausible.

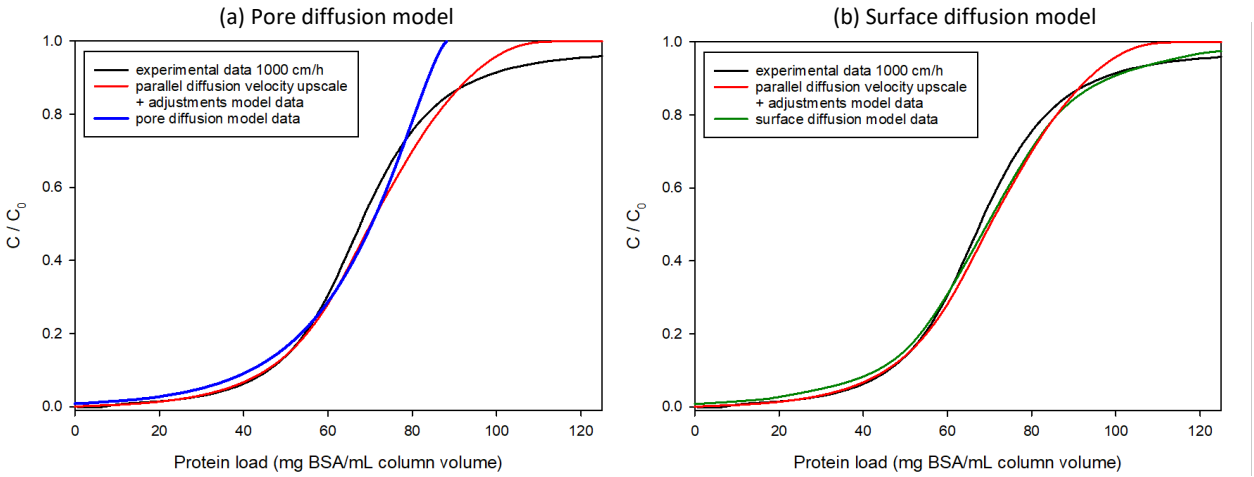

Figure 26: Iterative determined parallel diffusion model parameters in comparison with the pore and surface diffusion model versus the experimental data from Section 4.5 in weak buffer environment. All data was done with a linear velocity of 1000 cm/h and a protein feed concentration of 2 mg/mL.

Table 12: Fractogel weak binding buffer fitting parameters for 1000 cm/h experimental data from Section 4.5. The parallel diffusion fit parameters were generated through an iterative approach where the experimental data was fitted with the model until an acceptable fit was rendered. The pore and surface diffusion model parameters are from Section 4.6.1 as well as from Section 4.6.2 and depicted for purpose of comparison.

fitting method	D_e **(cm²/s)**	D_s **(cm²/s)**	q_m **(mg/ cm³particle)**
Parallel diffusion model	$8*10^{-7}$	$1*10^{-9}$	100
Pore diffusion model	$1*10^{-5}$	---	100
Surface diffusion model	---	$2.7*10^{-8}$	100

In conclusion it was possible to fit the weak buffer data far better and more precisely than its strong buffer equivalent. The method of finding results was the same in both cases. It was not possible to predetermine parameters for the Fractogel parallel diffusion parallel diffusion fit. The calculation and usage of the film mass transfer coefficient k_f however proved to be reliable and worthy to the cause. Parallel diffusion experiments with Toyopearl GigaCap Q-650M were not concluded as it opposes a structure like Fractogel EMD TMAE Hicap (M), therefore similar results were expected.

5 Conclusion

In this study, the intraparticle diffusion effects of BSA onto 4 different anion exchange-chromatographic resins (Q Sepharose Fast Flow, Q Ceramic HyperD F, Fractogel EMD TMAE Hicap (M) and Toyopearl GigaCap Q-650M) under different conditions were examined. It showed that using a strong binding buffer significantly increased the protein binding capacity on alle media due to a reduced ionic strength in combination with the 22 mM TRIS pH 8.1 used in the buffer. Q Sepharose Fast Flow operated dependent on the used buffer system, showed a change in the diffusion mechanism when switching the buffer systems. Under strong binding buffer conditions, surface diffusion was found to be the main mode of mass transfer, triggering an overall reduced solute uptake due to a reduced number of available pores for the mass transport under these conditions. With the weak binding buffer, it was revealed that the main mode of mass transportation was substituted by the pore diffusion mechanism. For the Q Ceramic HyperD F it was confirmed in accordance with selected literature that surface diffusion was the main driving force of mass transport. The rate of diffusion was independent of the buffer system used, for the strong binding buffer predictions based on the linear velocity u were completed successfully. Fractogel EMD TMAE Hicap (M) and Toyopearl GigaCap Q-650M, sharing a similar structure with the introduction of a grafted polymer onto a crosslinked polymethacrylate backbone, yielded similar results. During the process of chromatographic modelling, it became clear that both pore and surface diffusion offer contribution to the intraparticle adsorption of BSA onto these resins, resulting in a parallel diffusion mechanism. Due to the complexity of the calculations for the Fractogel EMD TMAE Hicap (M) parallel diffusion model, the parameter estimation for the 1000 cm/h velocity upscale was only possible by iterative fitting, a simple prediction was not successful.

Abbreviations

AIEX	Anion exchange Chromatography
BSA	Bovine Serum Albumine
BTC	Breakthrough Curve
CADET	Chromatography Analysis and Design Toolkit
CV	Column Volume
DBC	Dynamic Binding Capacity
EMG	Exponentially Modified Gaussian
GRM	General Rate Model
HETP	Height Equivalent to a Theoretical Plate
IEC, IEX	Ion Exchange Chromatography
LC	Liquid Chromatography
MTZ	Mass Transfer Zone
PBS	Phosphate Buffered Saline
RT	Room temperature
SEC	Size Exclusion Chromatography
SMA	Steric Mass Action
TRIS	Tris(hydroxymethyl)aminomethane

Nomenclature

$\widehat{D_e}$	Apparent effective pore diffusivity; $m^2\ s^{-1}$
A	Adsorption
Bi	Biot number
C	Concentration in mobile phase; mol m^{-3}
C_p	Concentration of solute in the bulk fluid; mol m^{-3}
$C_{p,\,i}$	Solute concentration in the pore liquid; mol m^{-3}
$C_{p,\,s}$	Protein concentration on the particle surface; mol m^{-3}
D_0	Free solution diffusivity; $m^2\ s^{-1}$
D_{ax}	Axial dispersion; $m^2\ s^{-1}$
D_e	Effective pore diffusivity; $m^2\ s^{-1}$
D_p	Pore diffusion coefficient; $m^2\ s^{-1}$
d_p	Particle diameter; m
D_s	Solid phase diffusion coefficient; $m^2\ s^{-1}$
F	Dimensionless fractional equilibrium
J	Mass transfer flux
K	Adsorption constant; m^3 kg
k_B	Boltzmann constant; $m^2\ g\ s^{-2}\ K^{-1}$
K_e	Dimensionless equilibrium constant
k_f	Film mass transfer coefficient; m s
l	Column length; m
l_c	Length of the cuvette; m
M_r	Molecular mass; Da
N_{film}	Number of transfer units onto the film
$N_{pore,f}$	Number of transfer units in the pore
Q	Volumetric flow rate; $m^3\ sec^{-1}$
q	Concentration of solute adsorbed on stationary phase; mol m^{-3}
q_0	Total ionic capacity of AIEX resin; mol m^{-3}
q_{max}	Maximum adsorbed solute concentration on stationary phase in Langmuir adsorption isotherm; mol m^{-3}
R	Dimensionless separation factor

Re	Reynolds number
r_h	Hydrodynamic protein radius; nm
r_p	Particle radius; m
r_{pore}	Resin pore radius; nm
Sc	Schmidt number
T	Temperature; K
t	Time; sec
t_{abs}	Absolute time; sec
t_{scale}	Time for scale
u	Linear flow velocity; m sec^{-1}
V	Volume; m^3
V	Solution Volume; m^3
V_M	Resin volume; m^3
V_P	Particle resin volume; m^3
z	Protein effective charge

Greek symbols

∇_c	Protein concentration gradient
δ	Diffusion resistance parameter
ε	Void fraction
ε	Extra-particle porosity
ε_A	Molar absorption coefficient; L $M^{-1}cm^{-1}$
ε_p	Intra-particle porosity
ε_t	Total column porosity
ζ	Bed length parameter
η	Dynamic viscosity; kg m^{-1} s^{-1}
λ_m	Ratio protein to pore radius
ν	Kinematc viscosity; m^2 s^{-1}
ρ	Density, kg m^3
σ	Shielding constant
τ	Time parameter

τ_P	Tortuosity factor
ϕ	Phase ratio
ψ_P	Diffusional hindrance coefficient

References

List of Figures

List of Tables

Literature

[1] D. K. Martin, O. Vicente, T. Beccari, M. Kellermayer, M. Koller, R. Lal, R. S. Marks, I. Marova, A. Mechler, D. Tapaloaga, P. Žnidaršič-Plazl, M. Dundar, A brief overview of global biotechnology, *Biotechnology and Biotechnological Equipment*. **35**, 354-363 (2021)

[2] N. F. Gordon, C. M. V. Moore, C. L. Cooney, An overview of continuous protein purification processes, *Biotechnology Advances*. **8**, 741-762 (1990)

[3] S. Zhang, T. Iskra, W. Daniels, J. Salm, C. Gallo, R. Godavarti, G. Carta, Structural and performance characteristics of representative anion exchange resins used for weak partitioning chromatography, *Biotechnology Progress*. **33**, 425-434 (2017)

[4] G. Carta, A. Jungbauer, *Protein Chromatography: Process Development and Scale-Up*, Wiley. (2010)

[5] P. R. Brown, E. Grushka, S. Lunte, *Advances in chromatography*, 1st editio edition, CRC Press. (2004)

[6] A. M. Lenhoff, Protein adsorption and transport in polymer-functionalized ion-exchangers, *Journal of Chromatography A*. **1218**, 8748-8759 (2011)

[7] L. Yu, Y. Sun, Recent advances in protein chromatography with polymer-grafted media, *Journal of Chromatography A*. **1638**, (2021)

[8] K. Cook, D. S. Kyle, S. Cubbon, Advances in Chromatography for Charge Variant Profiling of Biopharmaceuticals, in 28-32 (2017)

[9] D. Sunday, S. Curras-Medina, D. L. Green, Impact of initiator spacer length on grafting polystyrene from silica nanoparticles, *Macromolecules*. **43**, 4871-4878 (2010)

[10] J. A. V. Butler, C. Ockrent, Studies in Electrocapillarity. III, *The Journal of Physical Chemistry*. **34**, 2841-2859 (1930)

[11] E. C. Markham, A. F. Benton, THE ADSORPTION OF GAS MIXTURES BY SILICA, *Journal of the American Chemical Society*. **53**, 497-507 (1931)

[12] C. A. Brooks, S. M. Cramer, Steric mass-action ion exchange: Displacement profiles and induced salt gradients, *AIChE Journal*. **38**, 1969-1978 (1992)

[13] U. Altenhöner, M. Meurer, J. Strube, H. Schmidt-Traub, Parameter estimation for the simulation of liquid chromatography, *Journal of Chromatography A*. **769**, 59-69 (1997)

[14] G. Guiochon, A. Felinger, D. G. Shirazi, *Fundamentals of Preparative and Nonlinear Chromatography*, 2nd edition, Elsevier Academic Press. (2006)

[15] J. C. Bellot, J. S. Condoret, Modelling of liquid chromatography equilibria, *Process Biochemistry*. **28**, 365-376 (1993)

[16] T. Gu, G. Iyer, K.-S. C. Cheng, Parameter estimation and rate model simulation of partial breakthrough of bovine serum albumin on a column packed with large Q Sepharose anion-exchange particles, *Separation and Purification Technology*. **116**, 319-326 (2013)

[17] R. D. Whitley, X. Zhang, N. H. L. Wang, Protein denaturation in nonlinear isocratic and gradient elution chromatography, *AIChE Journal*. **40**, 1067-1081 (1994)

[18] E. von Lieres, J. Andersson, A fast and accurate solver for the general rate model of column liquid chromatography, *Computers and Chemical Engineering*. **34**, 1180-1191 (2010)

[19] J. Xu, L. Zhu, G. Xu, W. Yu, A. K. Ray, Determination of competitive adsorption isotherm of enantiomers on preparative chromatographic columns using inverse method, *Journal of Chromatography A*. **1273**, 49-56 (2013)

[20] P. Forssén, R. Arnell, T. Fornstedt, An improved algorithm for solving inverse problems in liquid chromatography, *Computers & Chemical Engineering*. **30**, 1381-1391 (2006)

[21] J. J. Carberry, A boundary-layer model of fluid-particle mass transfer in fixed beds, *AIChE Journal*. **6**, 460-463 (1960)

[22] H. Brenner, L. J. Gaydos, The constrained brownian movement of spherical particles in cylindrical pores of comparable radius: Models of the diffusive and convective transport of

solute molecules in membranes and porous media, *Journal of Colloid and Interface Science*. **58**, 312-356 (1977)
[23] J. L. Anderson, J. A. Quinn, Restricted transport in small pores. A model for steric exclusion and hindered particle motion, *Biophys J*. **14**, 130-150 (1974)
[24] R. B. Bird, W. E. Stewart, E. N. Lightfoot, Transport phenomena, *AIChE Journal*. **7**, 5J-6J (1961)
[25] M. T. Tyn, T. W. Gusek, Prediction of diffusion coefficients of proteins, *Biotechnol Bioeng*. **35**, 327-338 (1990)
[26] T. W. Weber, R. K. Chakravorti, Pore and solid diffusion models for fixed-bed adsorbers, *AIChE Journal*. **20**, 228-238 (1974)
[27] G. Carta, A. R. Ubiera, T. M. Pabst, Protein mass transfer kinetics in ion exchange media: Measurements and interpretations, *Chemical Engineering and Technology*. **28**, 1252-1264 (2005)
[28] H. Yoshida, T. Kataoka, D. M. Ruthven, Analytical solution of the breakthrough curve for rectangular isotherm systems, *Chemical Engineering Science*. **39**, 1489-1497 (1984)
[29] L. E. Weaver, G. Carta, Protein adsorption on cation exchangers: Comparison of macroporous and gel-composite media, *Biotechnology Progress*. **12**, 342-355 (1996)
[30] T. Vermeulen, Theory for Irreversible and Constant-Pattern Solid Diffusion, *Industrial & Engineering Chemistry*. **45**, 1664-1670 (1953)
[31] F. Helfferich, M. S. Plesset, Ion exchange kinetics. A nonlinear diffusion problem, *The Journal of Chemical Physics*. **28**, 418-424 (1958)
[32] N. N. Nashaat, Iron Oxide Nanoadsorbents for Removal of Various Pollutants from Wastewater: An Overview, Bentham Science Publisher p. 81-118. (2012)
[33] B. D. Kelley, M. Switzer, P. Bastek, J. F. Kramarczyk, K. Molnar, T. Yu, J. Coffman, High-throughput screening of chromatographic separations: IV. Ion-exchange, *Biotechnology and Bioengineering*. **100**, 950-963 (2008)
[34] I. Savoy, *Der Einsatz von Radialflusssäulen im Capture-Schritt von Antikörperaufreinigungen*, Hochschulle Mannheim (2009)
[35] S. Leweke, E. von Lieres, Chromatography Analysis and Design Toolkit (CADET), *Computers and Chemical Engineering*. **113**, 274-294 (2018)
[36] *Superdex 75 10/300 GL and Superdex 200 10/300 GL high performance columns packing instructions*, by GE Healthcare Bio-Sciences AB, Uppsala, Sweden, p. 2. (2014)
[37] M. A. Fernandez, G. Carta, Characterization of protein adsorption by composite silica-polyacrylamide gel anion exchangers. I. Equilibrium and mass transfer in agitated contactors, *Journal of Chromatography A*. **746**, 169-183 (1996)
[38] M. A. Fernandez, W. S. Laughinghouse, G. Carta, Characterization of protein adsorption by composite silica-polyacrylamide gel anion exchangers. II. Mass transfer in packed columns and predictability of breakthrough behavior, *Journal of Chromatography A*. **746**, 185-198 (1996)
[39] A. K. Hunter, G. Carta, Protein adsorption on novel acrylamido-based polymeric ion-exchangers: III. Salt concentration effects and elution behavior, *Journal of Chromatography A*. **930**, 79-93 (2001)
[40] A. K. Hunter, G. Carta, Protein adsorption on novel acrylamido-based polymeric ion-exchangers: IV. Effects of protein size on adsorption capacity and rate, *Journal of Chromatography A*. **971**, 105-116 (2002)
[41] J. A. Roberts, G. Carta, Relationship between HETP measurements and breakthrough curves in short chromatography columns, *Biotechnology Progress*. **37**, 1-10 (2021)
[42] E. Müller, Comparison between mass transfer properties of weak-anion-exchange resins with graft-functionalized polymer layers and traditional ungrafted resins, *Journal of Chromatography A*. **1006**, 229-240 (2003)
[43] *Chromatographic process media catalog*, by TOSOH Bioscience, p. 42. (2018/2019)